Parallel Adaptive High-Order CFD Simulations Characterizing SOFIA Cavity Acoustics

Michael Barad
Applied Modeling & Simulation Branch
NASA Ames Research Center

Co-workers : Christoph Brehm and Cetin Kiris

Applied Modeling & Simulation Seminar Series,
NASA Ames Research Center, January 27, 2015

Outline

- Background/Motivation
- LAVA Solver
- SOFIA Simulation Setup
- General Flow Features
- Spectral Analysis
- Proper Orthogonal Decomposition Analysis
- Conclusions

Motivation

- Stratospheric Observatory for Infrared Astronomy (SOFIA)
  - 2.5 meter telescope mounted in open cavity of Boeing 747SP
  - SOFIA observations are made when aircraft is at 12-14 kilometers
- SOFIA imaging quality is degraded by:
  - Local refraction index within telescope line-of-sight that depends on density fluctuations in shear layer
  - Unsteady pressure field (acoustics) inside cavity can induce telescope vibrations
- High-fidelity unsteady simulations were needed to better understand density fluctuations in line-of-sight, and pressure field in cavity
- LAVA solver with Cartesian immersed boundaries selected due to:
  - Geometric complexity -> NO MANUAL VOLUME GRID GENERATION!!
  - Accuracy of interior discretization scheme -> HIGH SPECTRAL ACCURACY!!
  - HIGH PARALLEL SCALABILITY!!

Stratospheric Observatory for Infrared Astronomy (SOFIA) Geometry

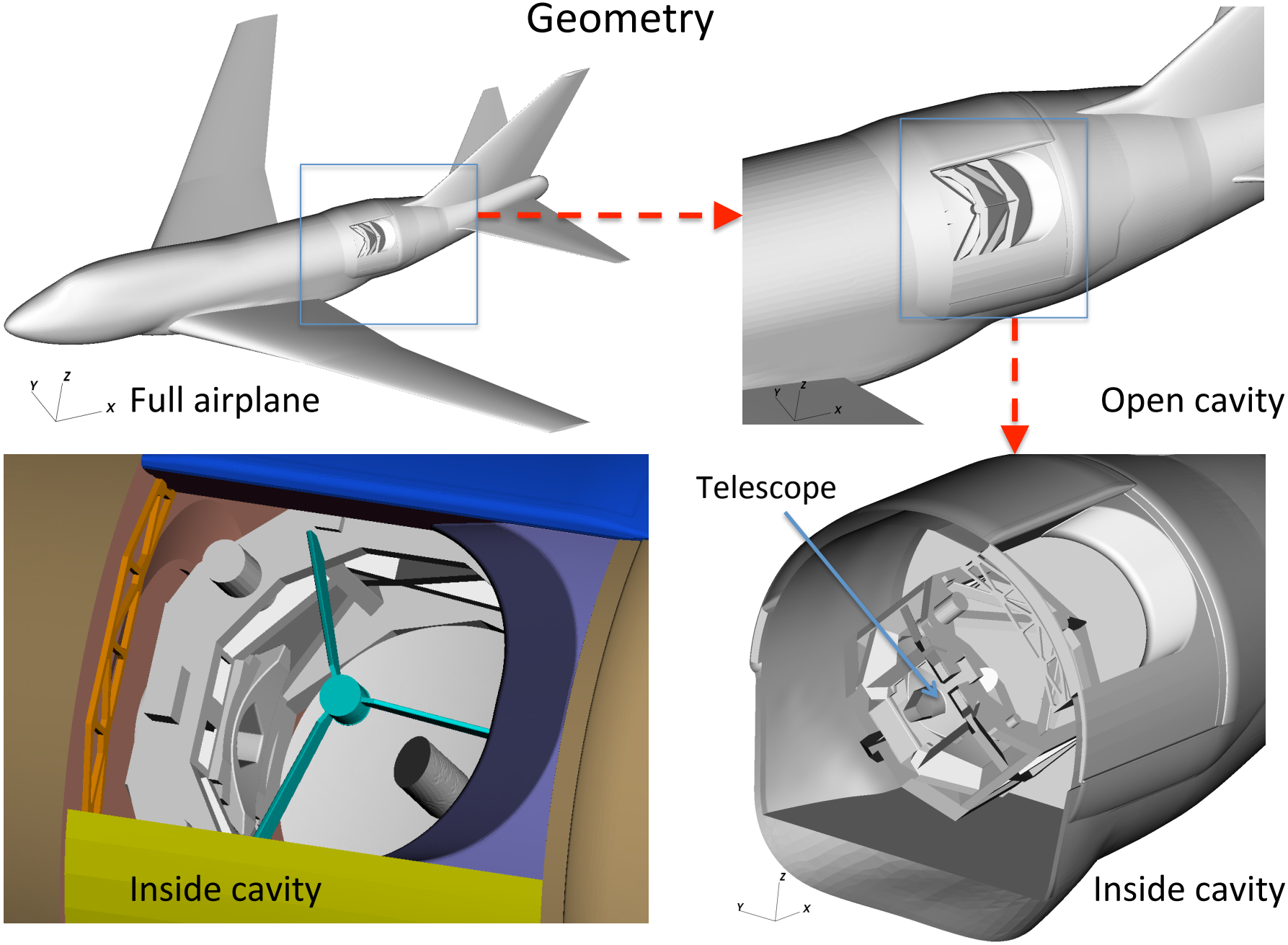

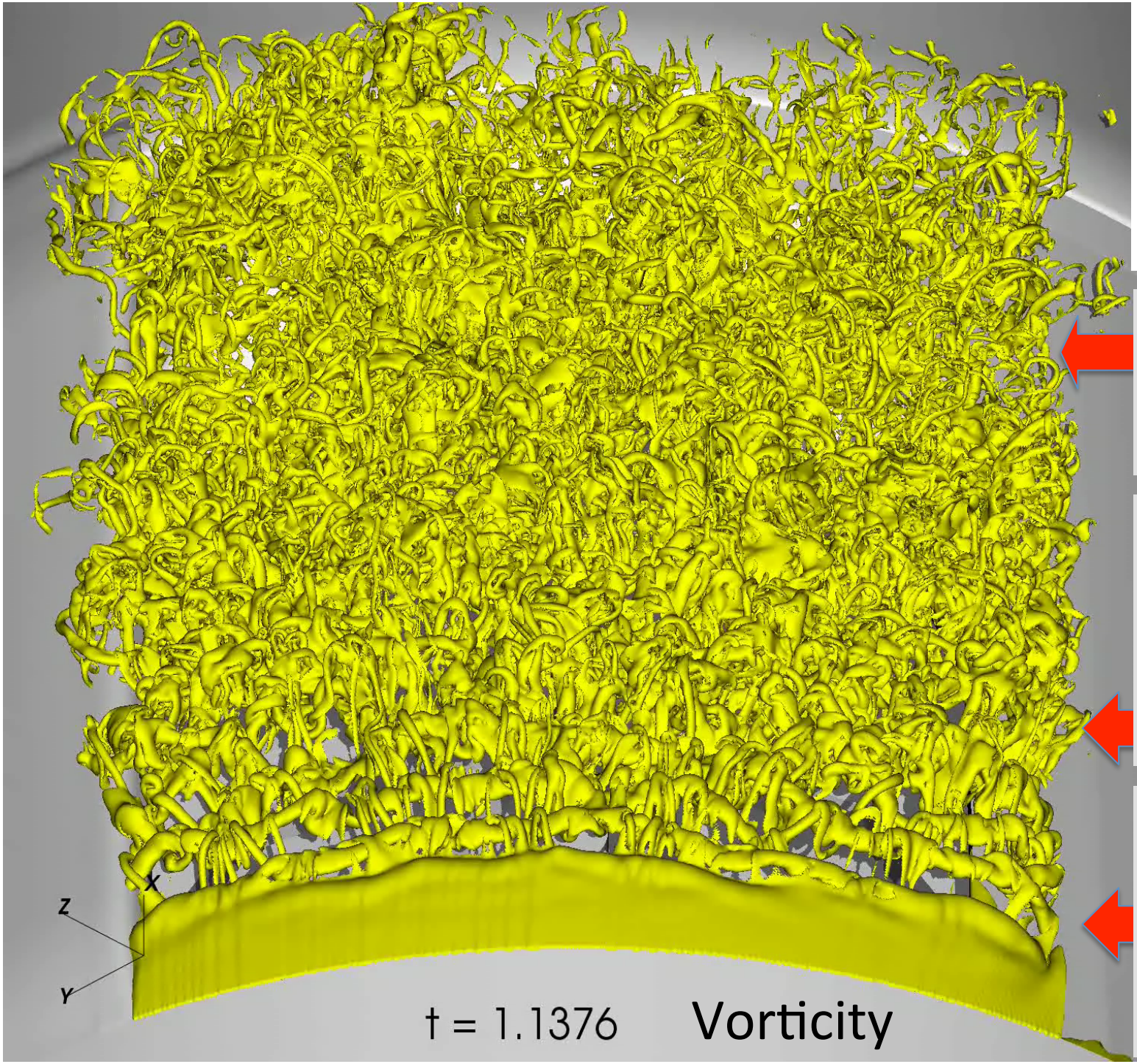

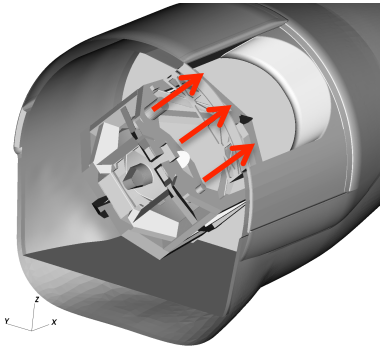

Fine scale vortices sweep across cavity opening.

Breakdown of coherent structures results in fine scale hairpin vortices.

Primary and secondary instabilities can be observed in the initial shear layer region.

Outline

- Background/Motivation
- LAVA Solver
- SOFIA Simulation Setup
- General Flow Features
- Spectral Analysis
- Proper Orthogonal Decomposition Analysis
- Conclusions

Launch Ascent & Vehicle Aerodynamics (LAVA)

- Highly flexible with respect to computational mesh
  - Block-structured Cartesian meshes with Adaptive Mesh Refinement (AMR) and Immersed-Boundary (IB)
  - Unstructured arbitrary polyhedral meshes
  - Structured curvilinear overset meshes
- Overset coupling of different mesh types

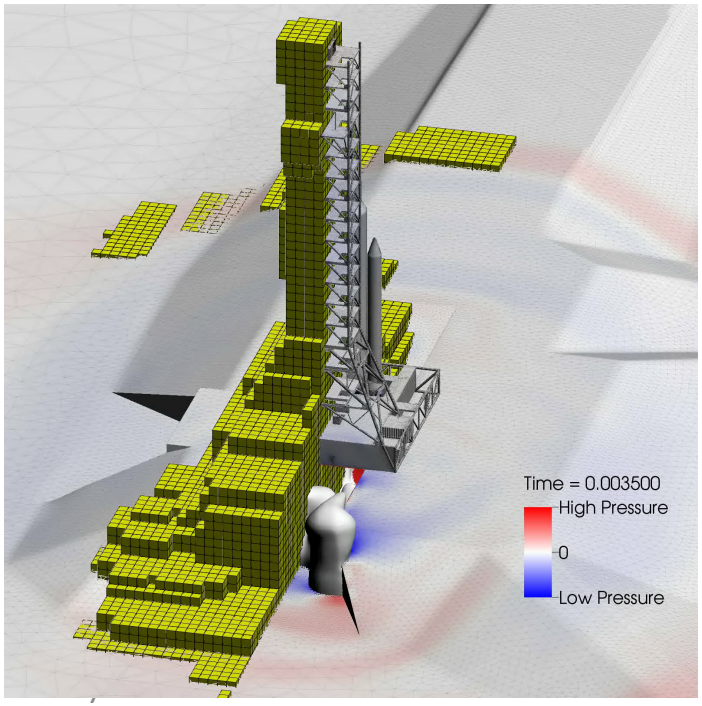

Cartesian AMR

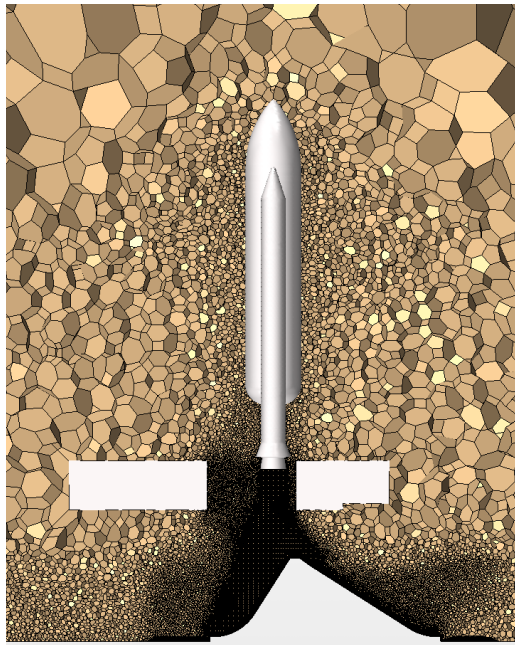

Unstructured Arbitrary Polyhedral

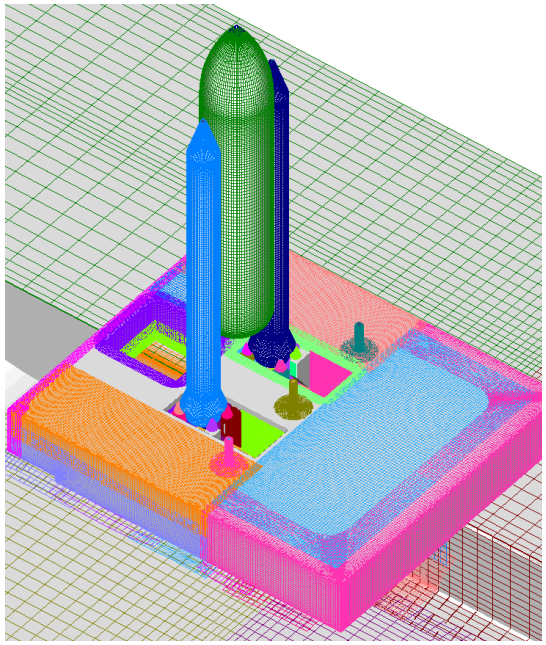

Overset Structured Curvilinear

Kiris, Barad, Housman, Sozer, Brehm, Moini-Yekta, AIAA 2014-0070
Brehm, Barad, Housman, Kiris, AIAA 2014-1278
Sozer, Brehm, Kiris, AIAA 2014-1440

LAVA Infrastructure Design

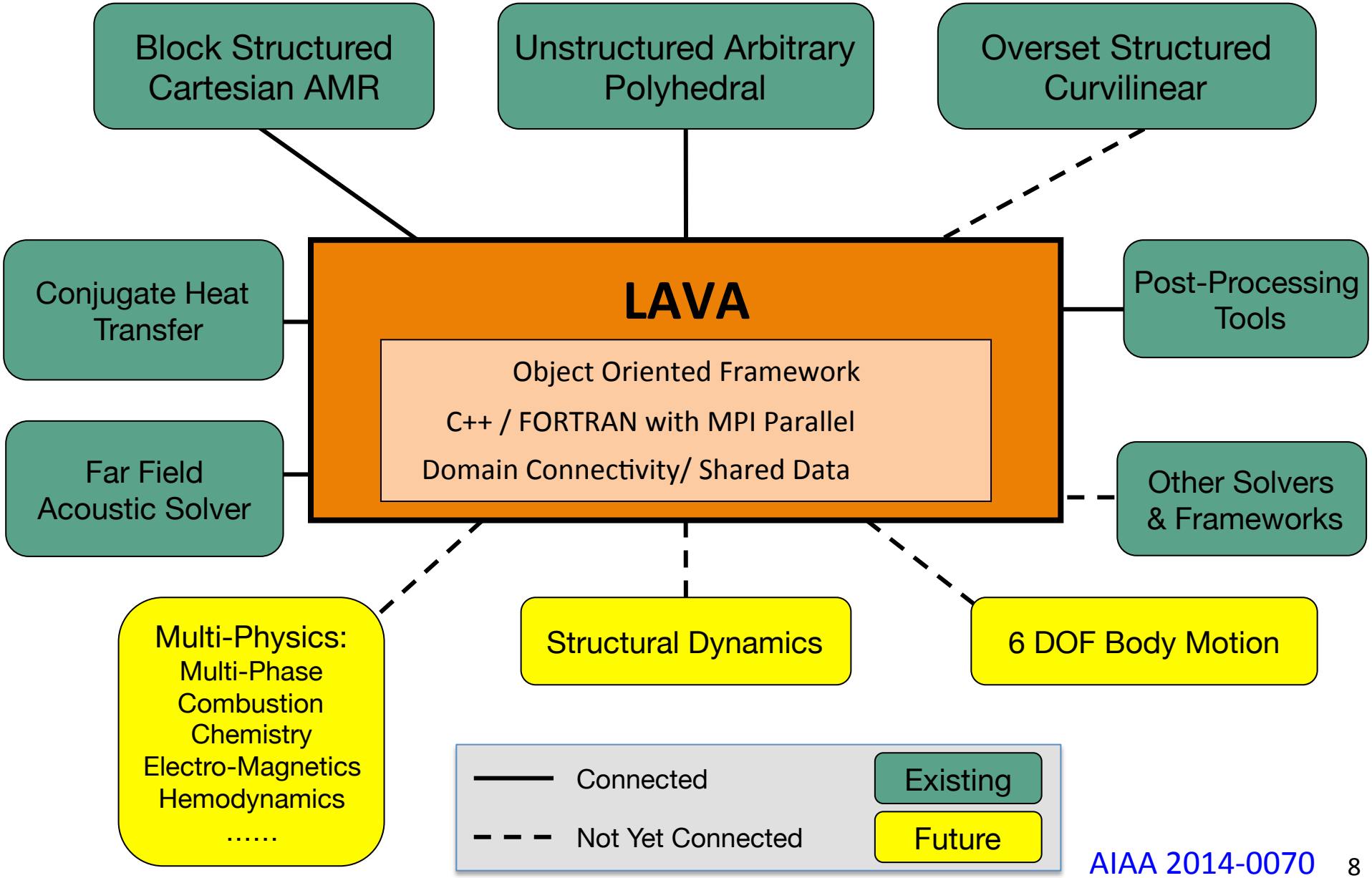

Block-Structured Cartesian

- Physics:
  - Compressible Navier-Stokes formulation
  - Multi-species formulation
  - SA and SST turbulence models and DES
- Numerics:
  - Higher-order spatial accuracy for convective terms (WENO, LAD, Central, etc) ***AIAA 2014-1278***
  - Time stepping options:
    - High-order explicit (Shu-Osher form)
    - Implicit with dual-time stepping
  - Preconditioning for low speed flows
  - Roe, AUSMPW+, central and van Leer convective flux formulations
  - Line relaxation linear solver for implicit
  - Parallel with MPI, uses Chombo
- Gridding:
  - Automatic volume grid generation requiring only a surface triangulation
  - Adaptive mesh refinement (AMR) for tracking flow features with local refinement (gradient, entropy adjoint, and geometry based)

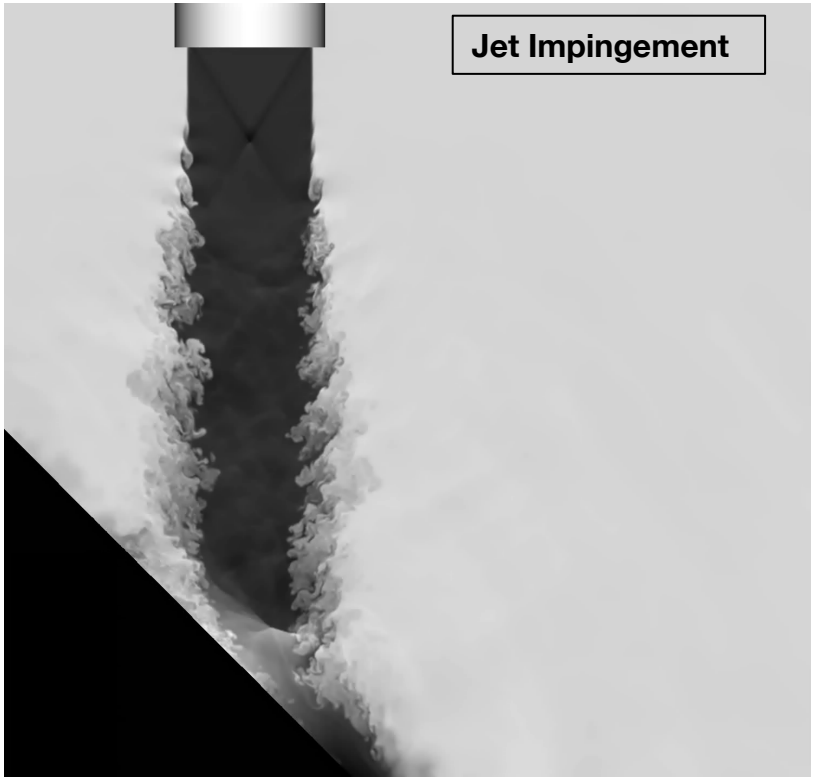

Block-Structured Cartesian

- Physics:
  - Compressible Navier-Stokes formulation
  - Multi-species formulation
  - SA and SST turbulence models and DES
- Numerics:
  - Higher-order spatial accuracy for convective terms (WENO, LAD, Central, etc) ***AIAA 2014-1278***
  - Time stepping options:
    - High-order explicit (Shu-Osher form)
    - Implicit with dual-time stepping
  - Preconditioning for low speed flows
  - Roe, AUSMPW+, central and van Leer convective flux formulations
  - Line relaxation linear solver for implicit
  - Parallel with MPI, uses Chombo
- Gridding:
  - Automatic volume grid generation requiring only a surface triangulation
  - Adaptive mesh refinement (AMR) for tracking flow features with local refinement (gradient, entropy adjoint, and geometry based)

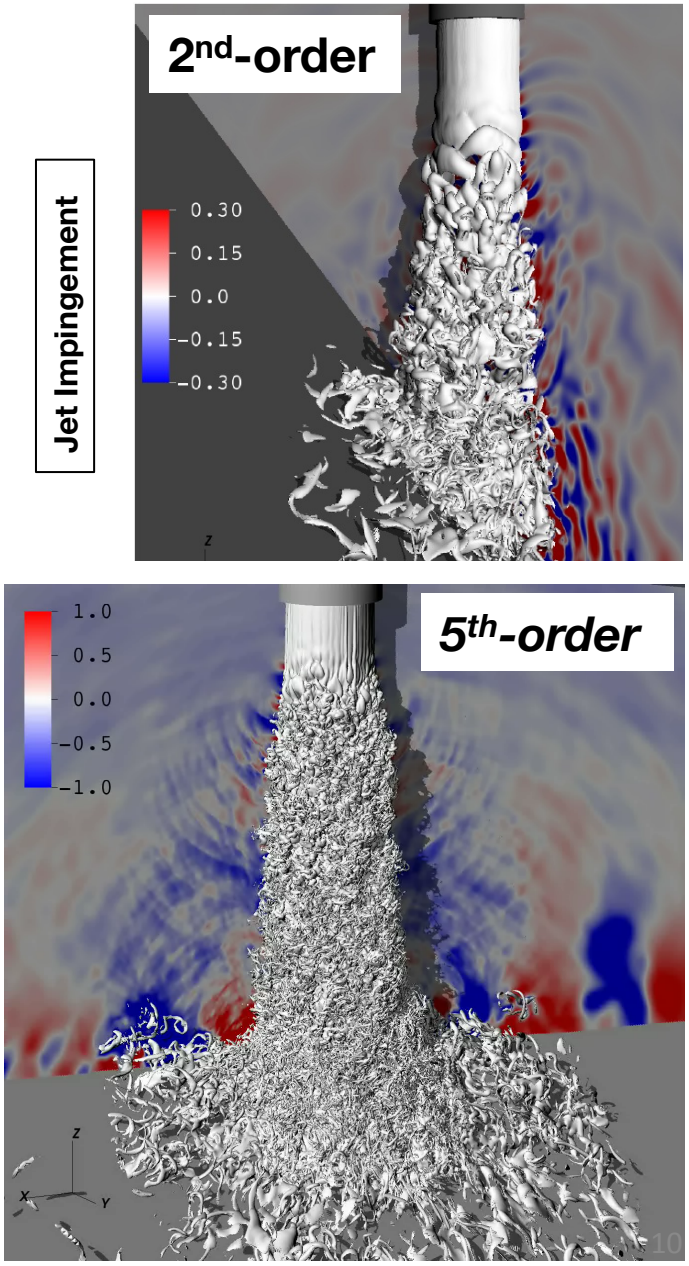

Block-Structured Cartesian

- Physics:
  - Compressible Navier-Stokes formulation
  - Multi-species formulation
  - SA and SST turbulence models and DES
- Numerics:
  - Higher-order spatial accuracy for convective terms (WENO, LAD, Central, etc) ***AIAA 2014-1278***
  - Time stepping options:
    - High-order explicit (Shu-Osher form)
    - Implicit with dual-time stepping
  - Preconditioning for low speed flows
  - Roe, AUSMPW+, central and van Leer convective flux formulations
  - Line relaxation linear solver for implicit
  - Parallel with MPI, uses Chombo
- Gridding:
  - Automatic volume grid generation requiring only a surface triangulation
  - Adaptive mesh refinement (AMR) for tracking flow features with local refinement (gradient, entropy adjoint, and geometry based)

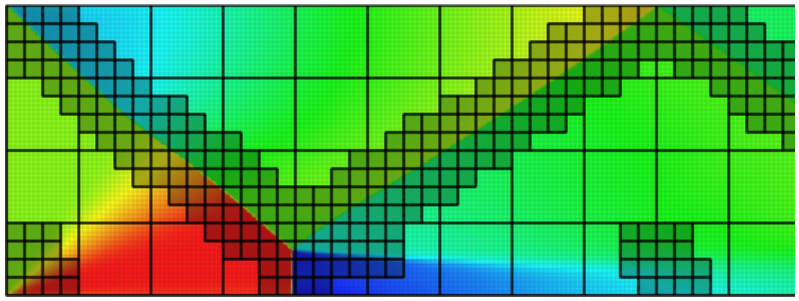

Shock Reflection in a Rectangular Channel

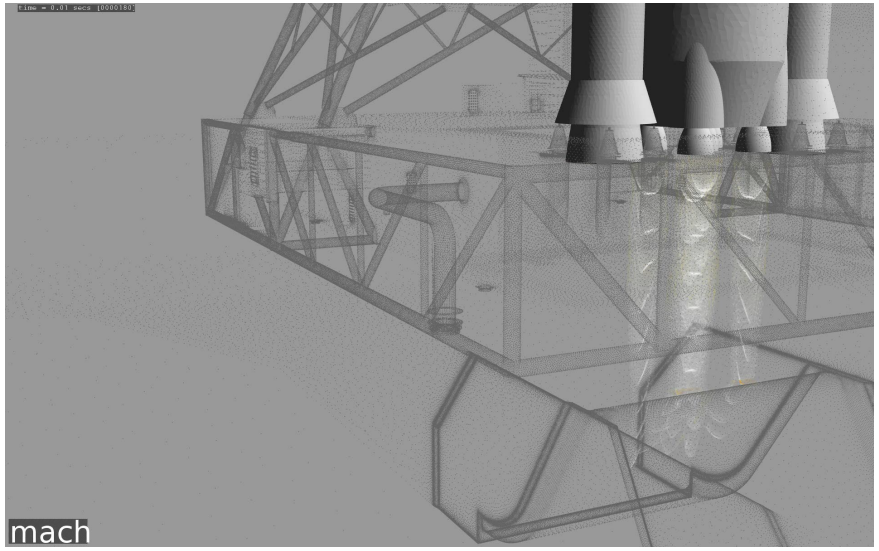

Arbitrarily Complex Geometry

Cartesian Immersed-Boundary

- Sharp interface immersed-boundary representation of geometry
- Image points at fixed distance
- Interpolation to image points from fluid interior (tri-linear or linear least-squares)
- Boundary condition imposed on “ghost cells”
- Fast parallel algorithms are implemented:
  - Inside-outside testing by multi-resolution binning
  - Exact distance to surface triangulation (including point to plane and point to edge cases)
- Excellent for highly complex geometry, and works well with AMR

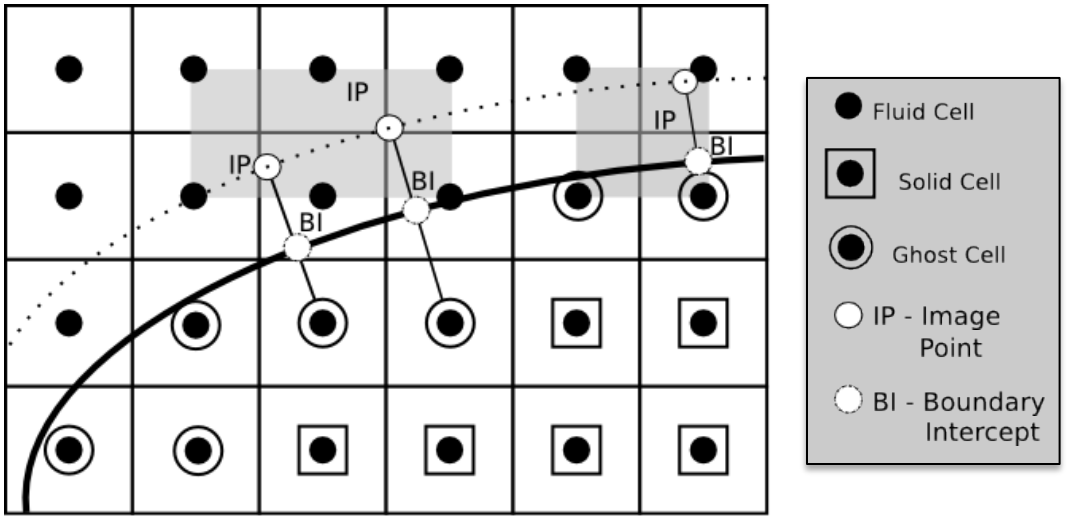

Fixed Distance

LAVA Validations: SLS Unsteady Ascent Aerodynamics

- Protuberances and attachment hardware may cause significant aerodynamic unsteadiness. Cyclical loads and an undesirable acoustic environment
- Rapid design analysis is possible with the Cartesian solver which eliminates time consuming mesh generation
- Comparison of LAVA results and experimental data focused on oscillatory wake region behind the SRB forward attachment.

NASA Langley Transonic Dynamics Tunnel (TDT) Test

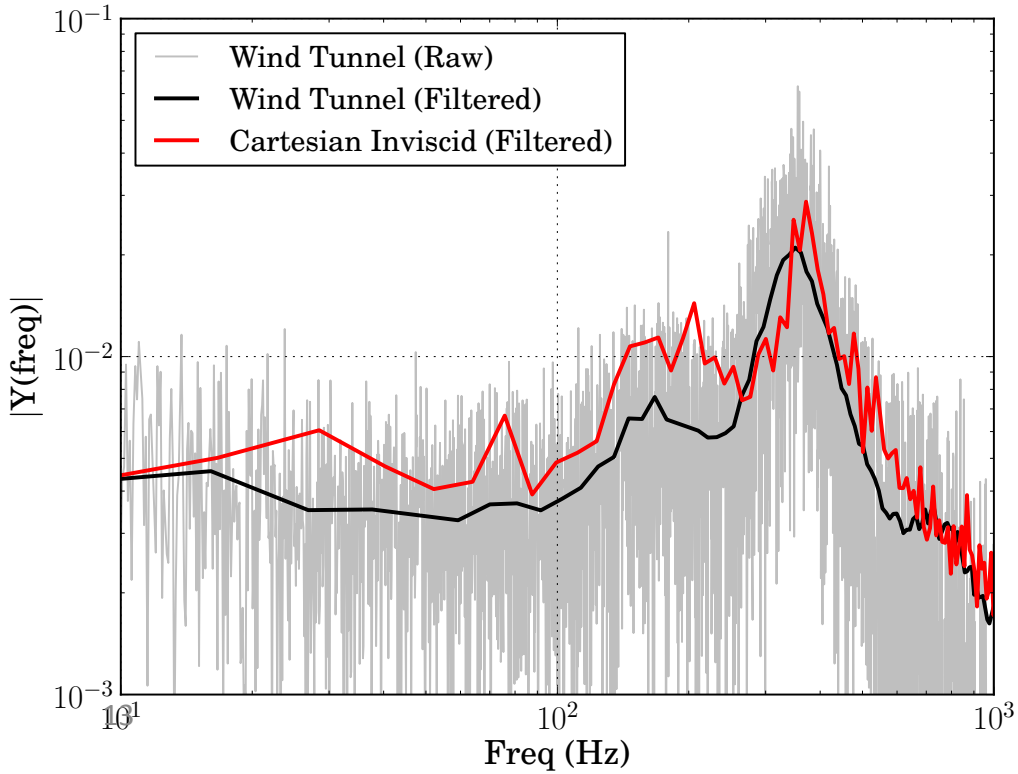

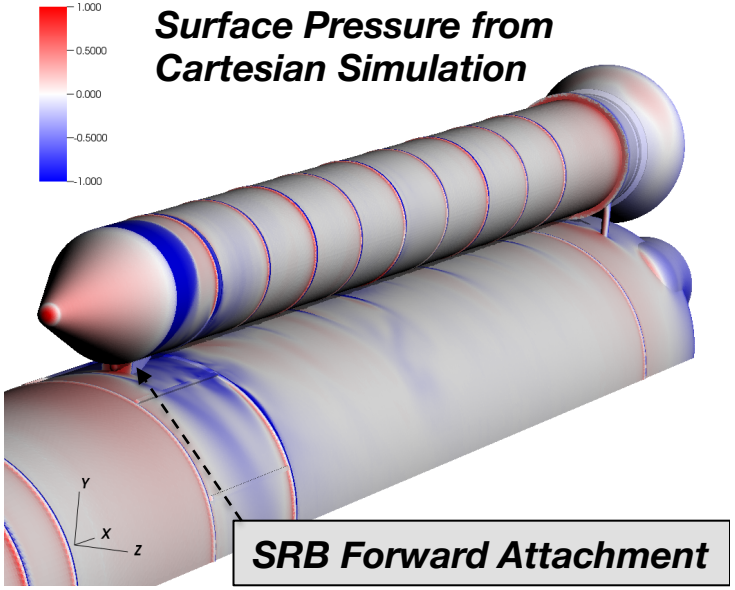

Surface Pressure from Cartesian Simulation

SRB Forward Attachment

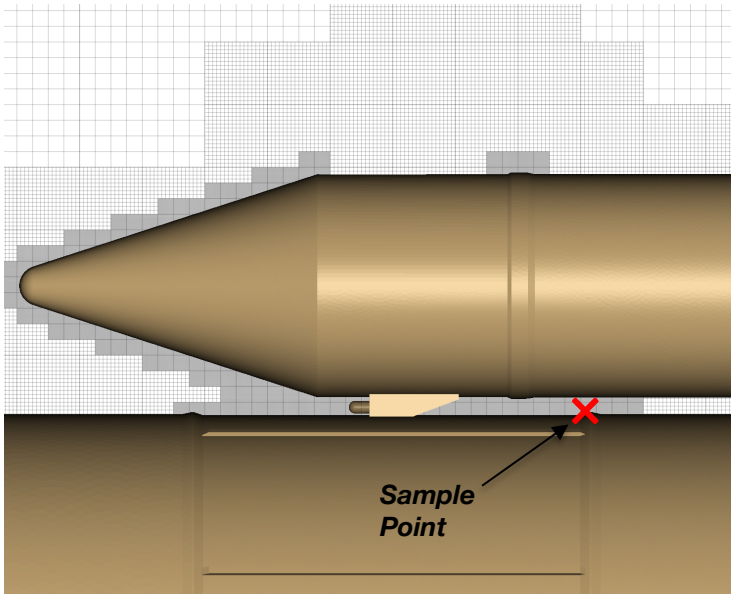

Kiris, Barad, Housman, Sozer, Brehm, Moini-Yekta, AIAA 2014-0070

LAVA Validations: AIAA BANC-III Test Case : Landing Gear

The LAVA solver was applied to a workshop Landing Gear problem

- Immersed-boundary (IB) utilized
  - Slip, no-slip, and wall modeled boundary conditions tested
  - Surface triangulation only requirement
- Higher-order accurate schemes
  - Fifth-order WENO Convection
  - 2nd order viscous (ILES)
  - 2nd order inter-level operators
- Time-accurate simulations
  - 4th order explicit RK
- Ffowcs William-Hawkings (FWH) noise propagation module

Mach = 0.166 Re = 73000	Uref = 56.3 m/s Tref = 286 K Pref = 99241 Pa

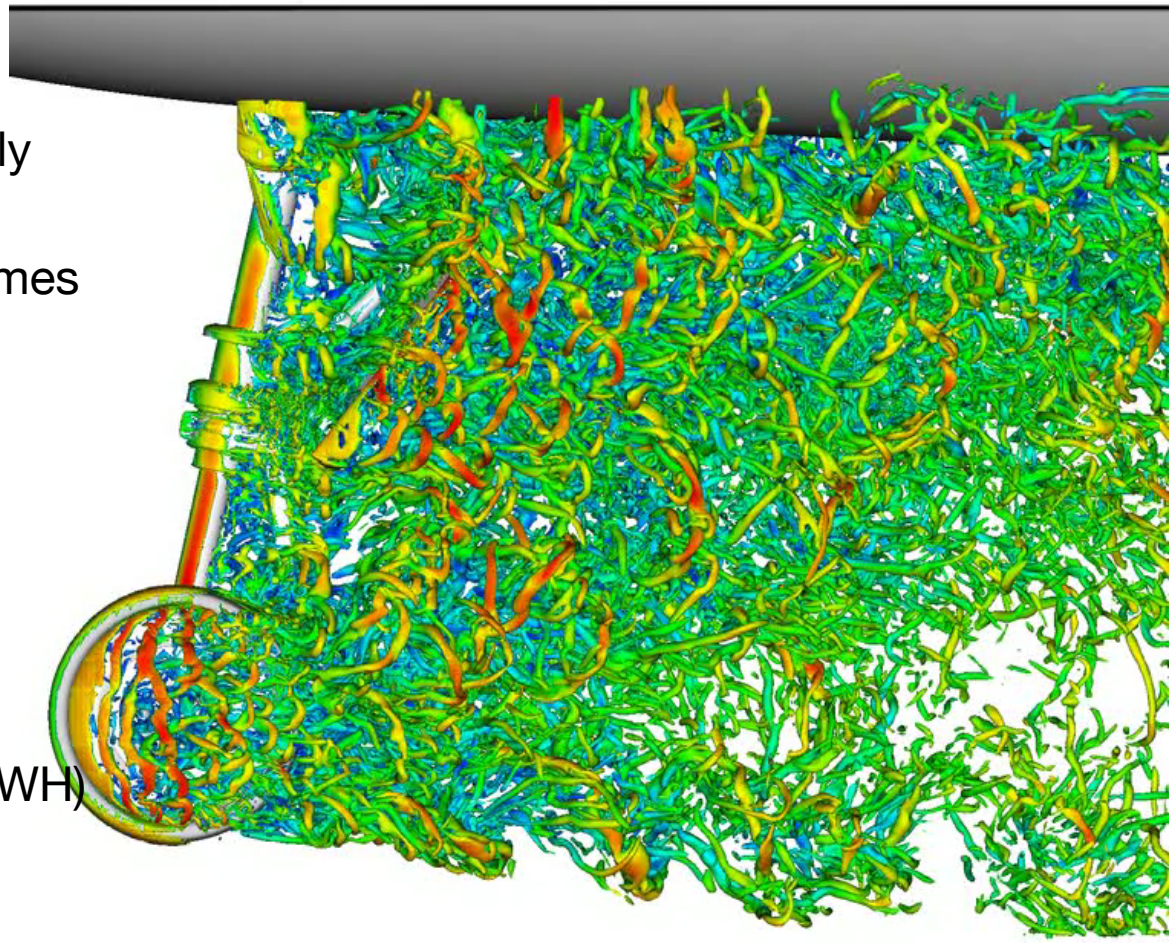

Moini-Yekta, Barad, Brehm, Housman, Kiris, AIAA BANC-III Workshop 2014

LAVA Validations: AIAA BANC-III Test Case : Landing Gear

Power Spectral Density of Pressure

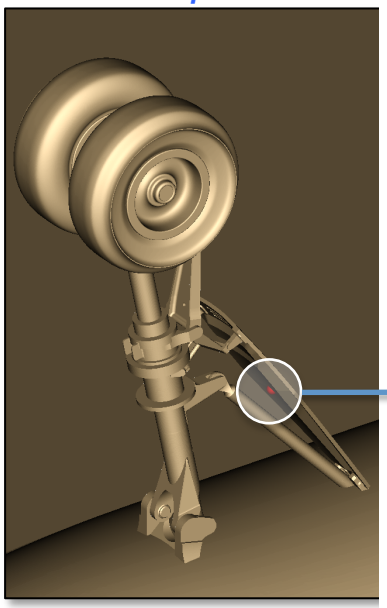

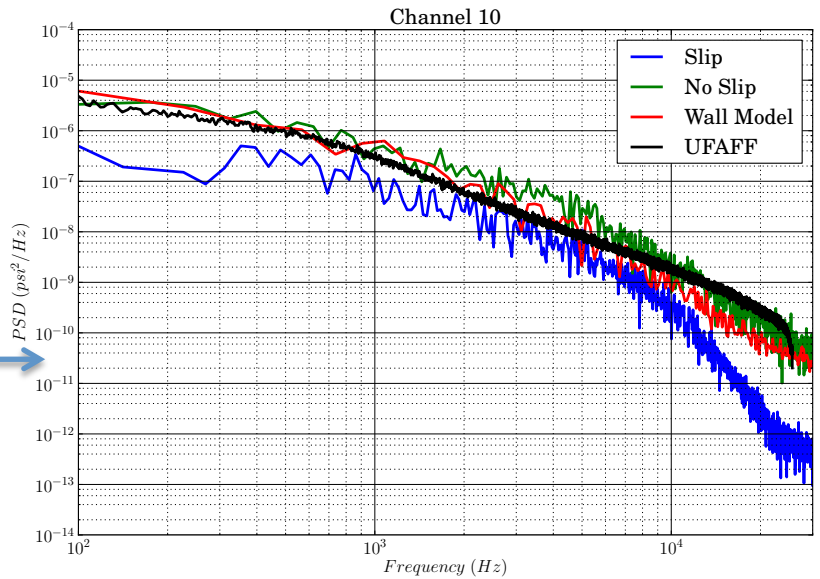

Far Field Acoustic SPL

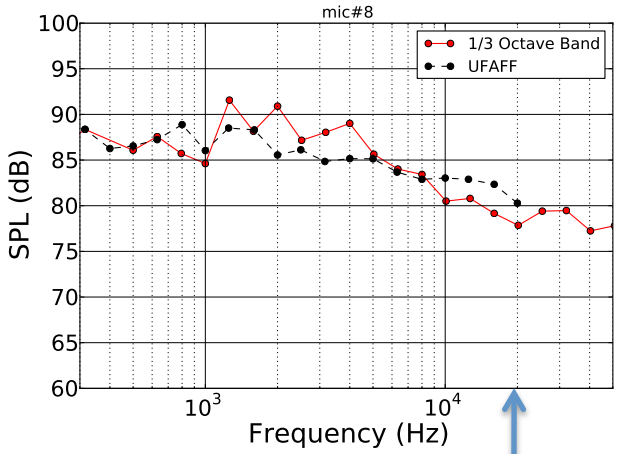

Ffowcs William-Hawkings (FWK) acoustic propagation LAVA module utilized

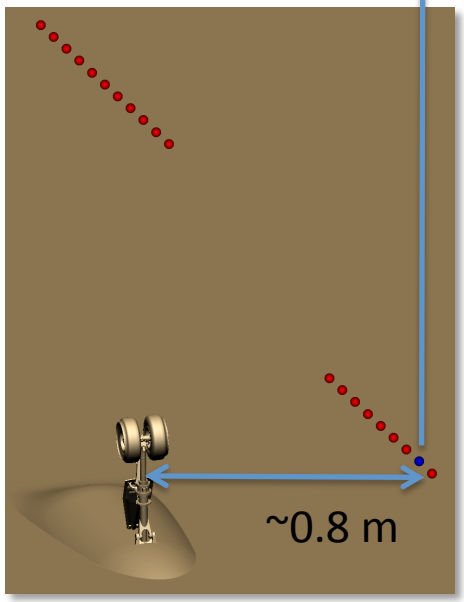

PIV Mean Turbulent Kinetic Energy Comparison

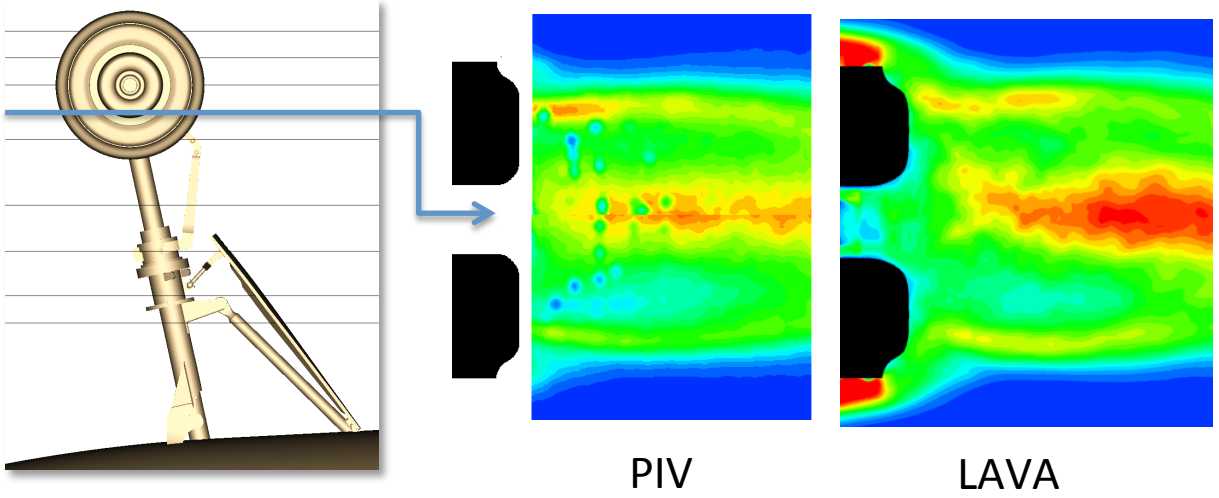

PIV LAVA

Outline

- Background/Motivation
- LAVA Solver
- SOFIA Simulation Setup
- General Flow Features
- Spectral Analysis
- Proper Orthogonal Decomposition Analysis
- Conclusions

Simulation Setup

- Flight conditions:

Mach = 0.88 Re = 5.25e6 per m	Uref = 259.7 m/s Tref = 216.7 K Pref = 17874 Pa

- Time Discretization: 4th order Explicit Runge-Kutta:

  dt = 6e-6 s, duration = 1.19 s (198000 steps).

- Space Discretization: 5th order WENO-5Z
  - Block-structured Cartesian
  - Immersed boundary
- ILES simulations focused on cavity flow, but whole vehicle is included

Automatic Volume Mesh Generation

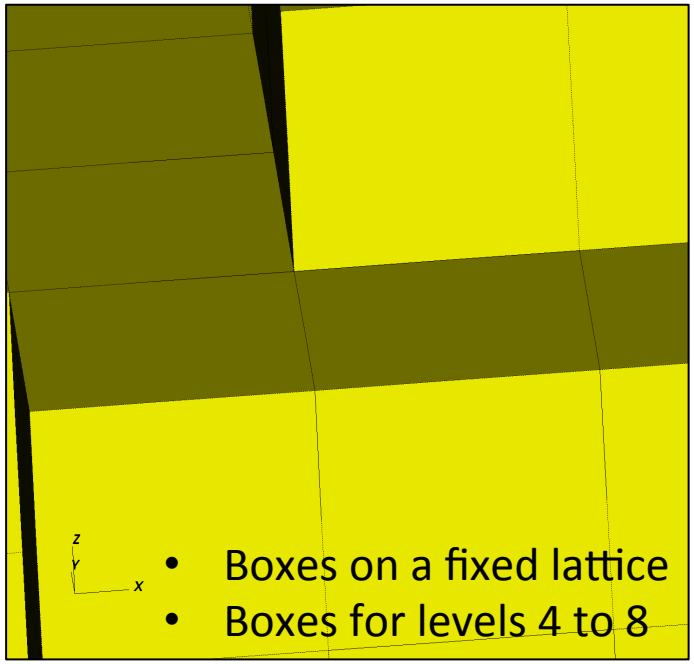

- Coarse mesh
  - 7 Levels
  - 173 million cells total
  - 24mm dx in shear layer and cavity
- Fine mesh
  - 8 Levels
  - 246 million cells total
  - 6mm dx in shear layer
  - 24mm dx in cavity

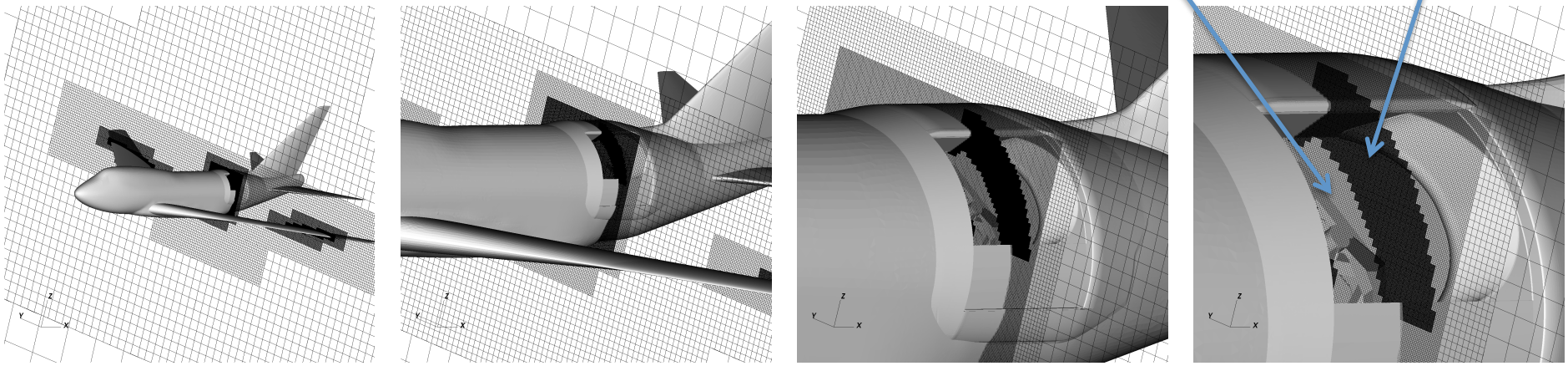

Fine mesh: 8 levels

SOFIA Simulations Overview

- Parallel scaling analysis performed
  - Identify limits to scaling
  - Test supercomputer system
  - Identify appropriate resources for flow analysis
- Coarse and fine unsteady ILES simulations have been performed
- Computed results were post-processed using:
  - Unsteady visualization
  - Point and surface spectral analysis
  - Proper Orthogonal Decomposition

Strong Parallel Scaling: Domain Decomposition

Mesh	Box Size	Number of Boxes	Number of Cells No Ghosts	Number of Cells With 3 Ghosts	(# With Ghosts)/(# No Ghosts)	Procs Used
Fine (8 levels)	8^3	392K	2.0×10^8	1.1×10^9	5.36	400 to 8K
Fine (8 levels)	16^3	60K	2.5×10^8	6.4×10^8	2.60	400 to 8K
Fine (8 levels)	32^3	10K	3.4×10^8	5.7×10^8	1.67	400 to 8K
Extra Fine (9 levels)	32^3	137K	4.4×10^9	7.5×10^9	1.67	6K to 32K

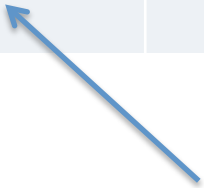

3 Ghosts: $(N+6)^3/N^3$

- For each fixed mesh, vary number of cores (i.e. strong scaling)
- Geometry based tagging used here
- Scaling study was performed for 25 time steps. 250M grid was used for the flow analysis.

Strong Parallel Scaling: Algorithm Decomposition

	Entire RK-solve including communication	WENO-5Z flux and divergence operators	Immersed boundary conditions
300 million cells (fine mesh)	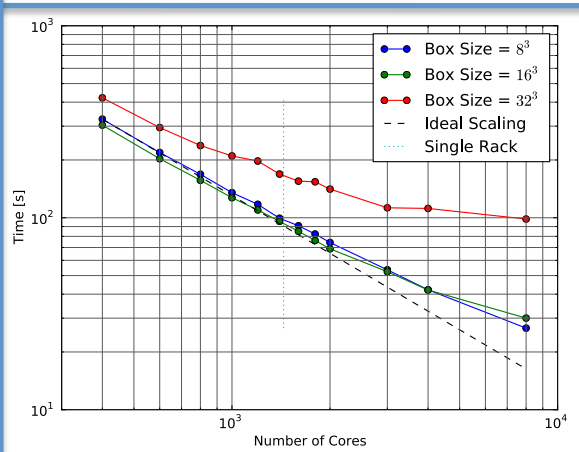	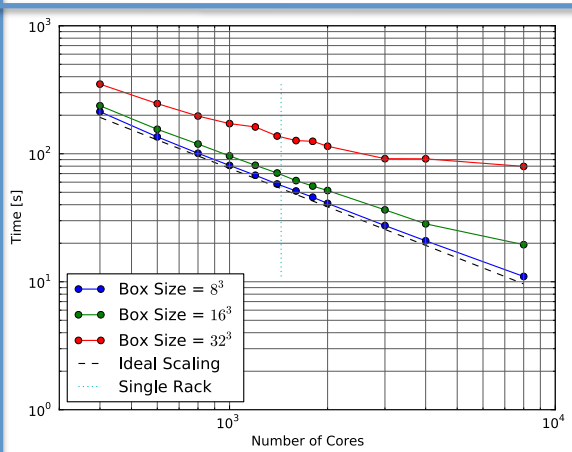	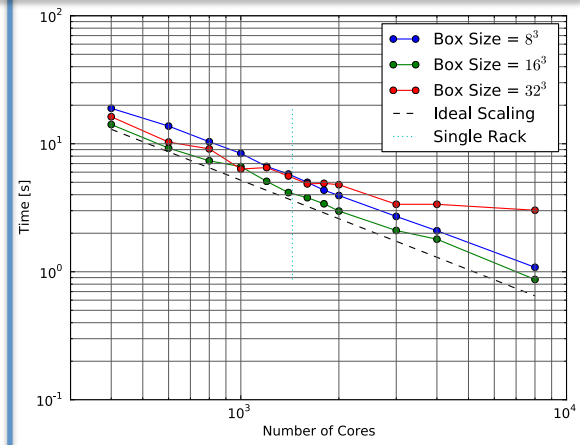
4.4 billion cells (super-fine mesh)	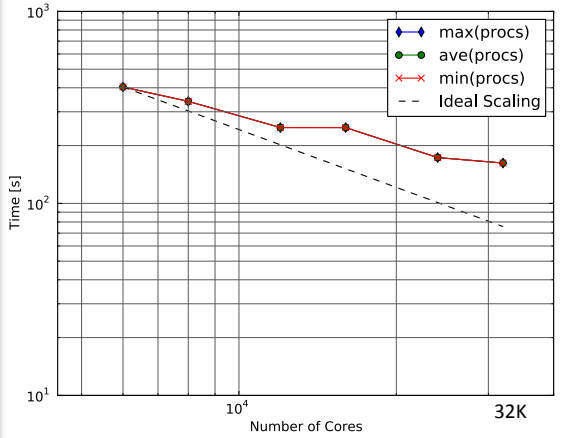	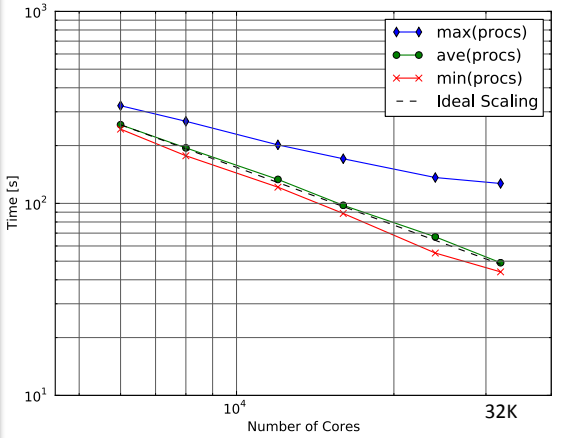	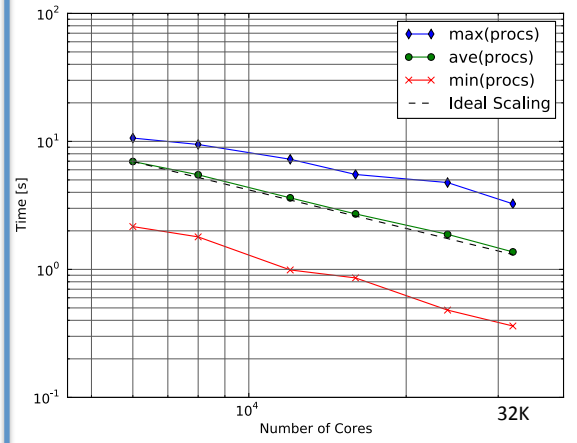

Strong parallel scaling study for 25 time steps:

- Top row is max time over all procs
- Bottom row is min/ave/max time over all procs shown for box size of 32^3

Super-fine mesh, boxes per level = [8,8,12,52,474,7K,4K, 126K]. Load balance issue @ 32^3:

- Fix 1: Multi-level load balance (i.e. 137K/32K)
- Fix 2: Hybrid MPI/OpenMP for node based balancing
- Fix 3: Mesh meta-data compression (16^3 -> ~1e6 boxes -> memory!)

Strong Parallel Scaling:
Dynamic Load Balancing with Mesh Adaption

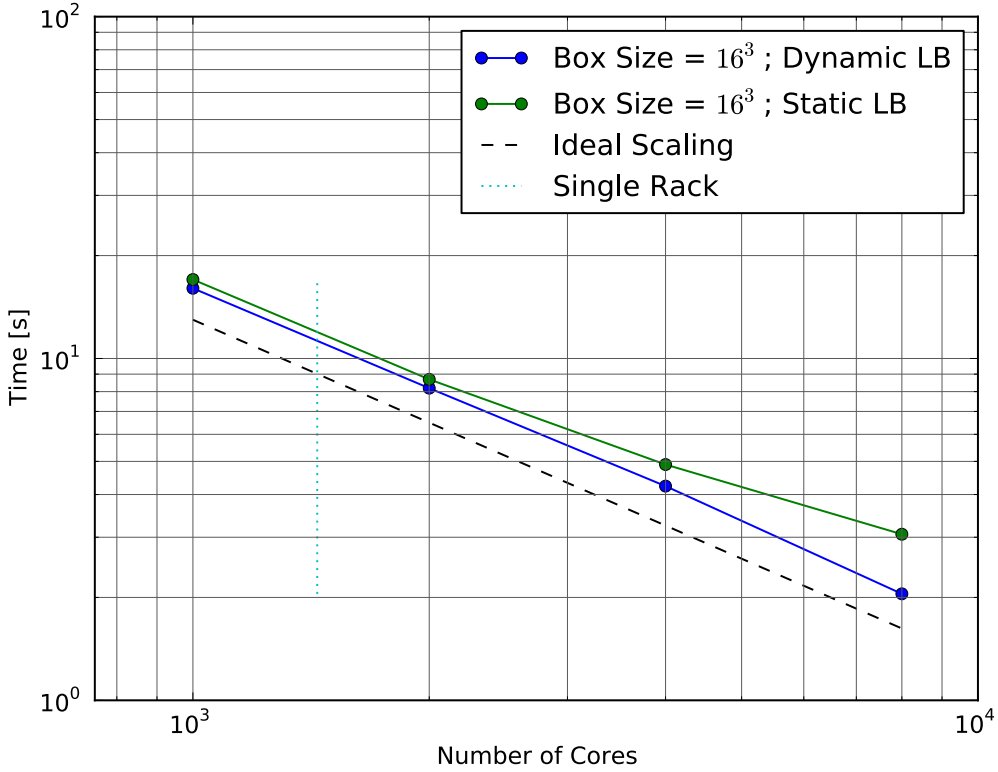

- Strong parallel scaling study for 100 time steps, adaptively regridding every 5 steps, comparing dynamic and static load balancing schemes.
  - 300 million cell mesh, with max time over all procs shown.
  - Timings are for immersed boundary conditions routines only, using box size of 16^3.
- Lattice of boxes is used for dynamic load balancing. Cost per box is stored and used during regrid.

Outline

- Background/Motivation
- LAVA Solver
- SOFIA Simulation Setup
- General Flow Features
- Spectral Analysis
- Proper Orthogonal Decomposition Analysis
- Conclusions

Cutting planes and mesh

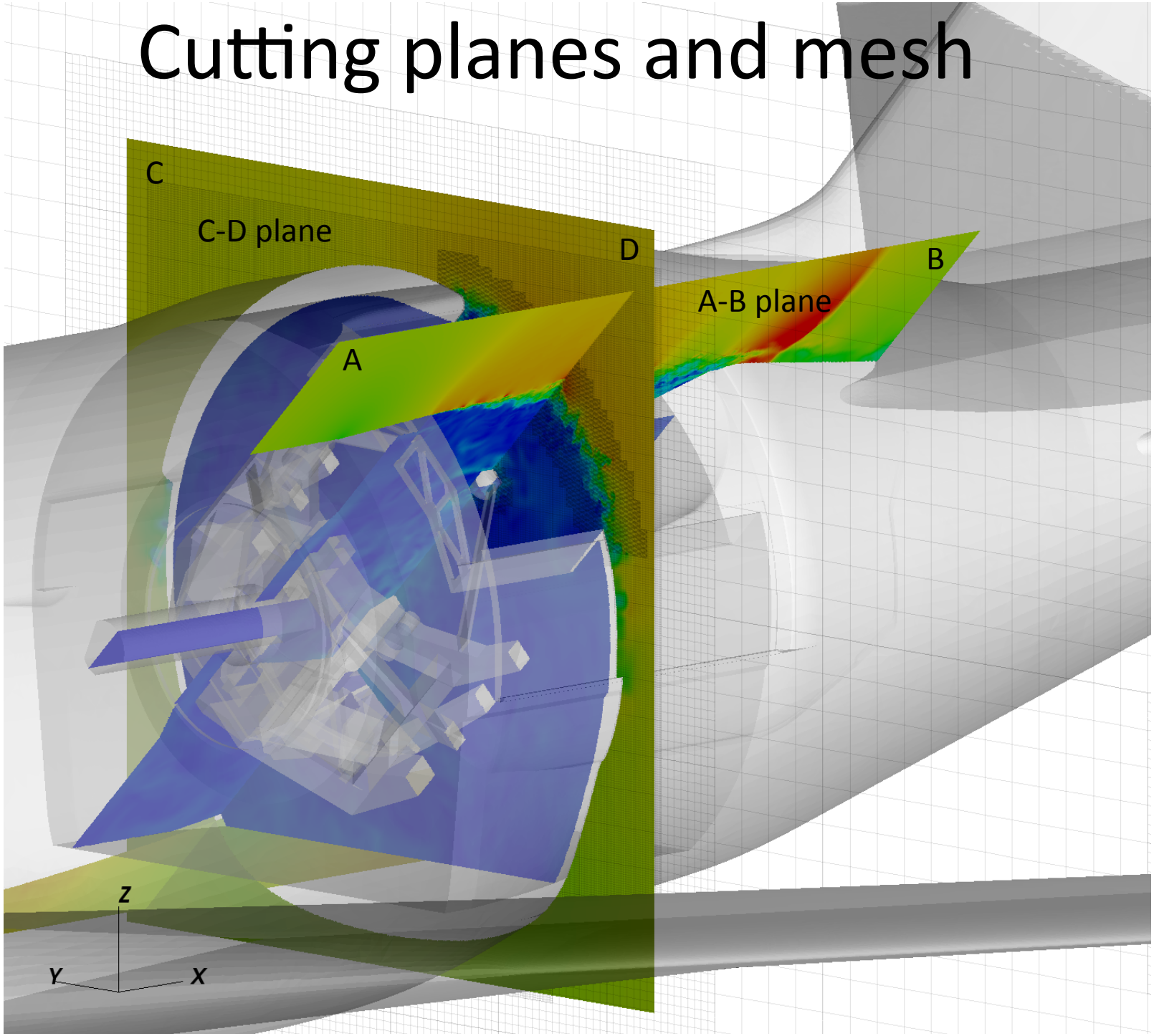

Coarse Shear Layer Grid

(A-B Plane)

Contours show development of unsteady shear layer and low-speed unsteady cavity circulation. Also apparent are acoustic waves.

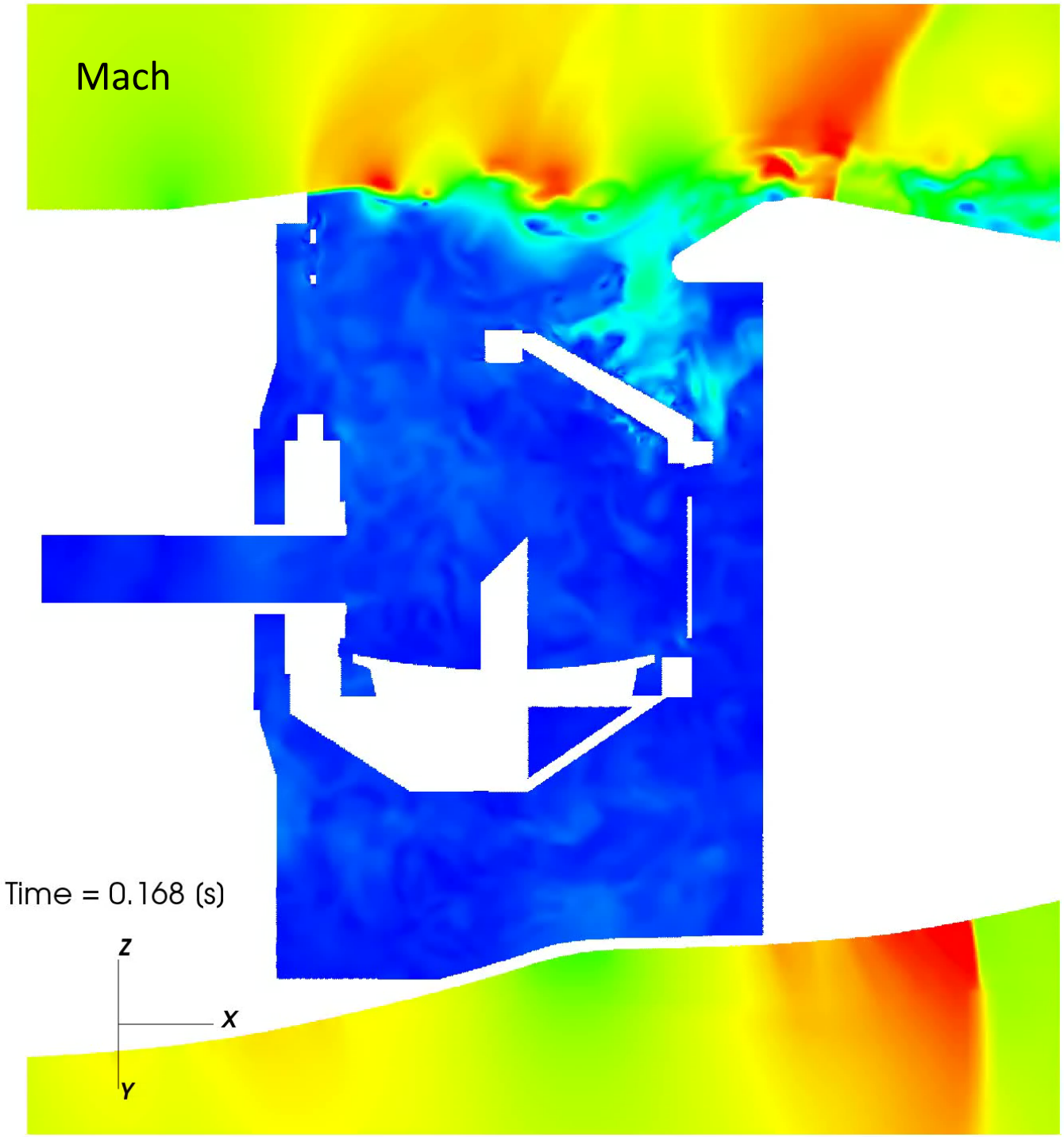

Fine Shear Layer Grid

(A-B Plane)

Simulation with refined mesh shows earlier breakup of the shear layer, reducing size of vortical structures and reduced shock interaction.

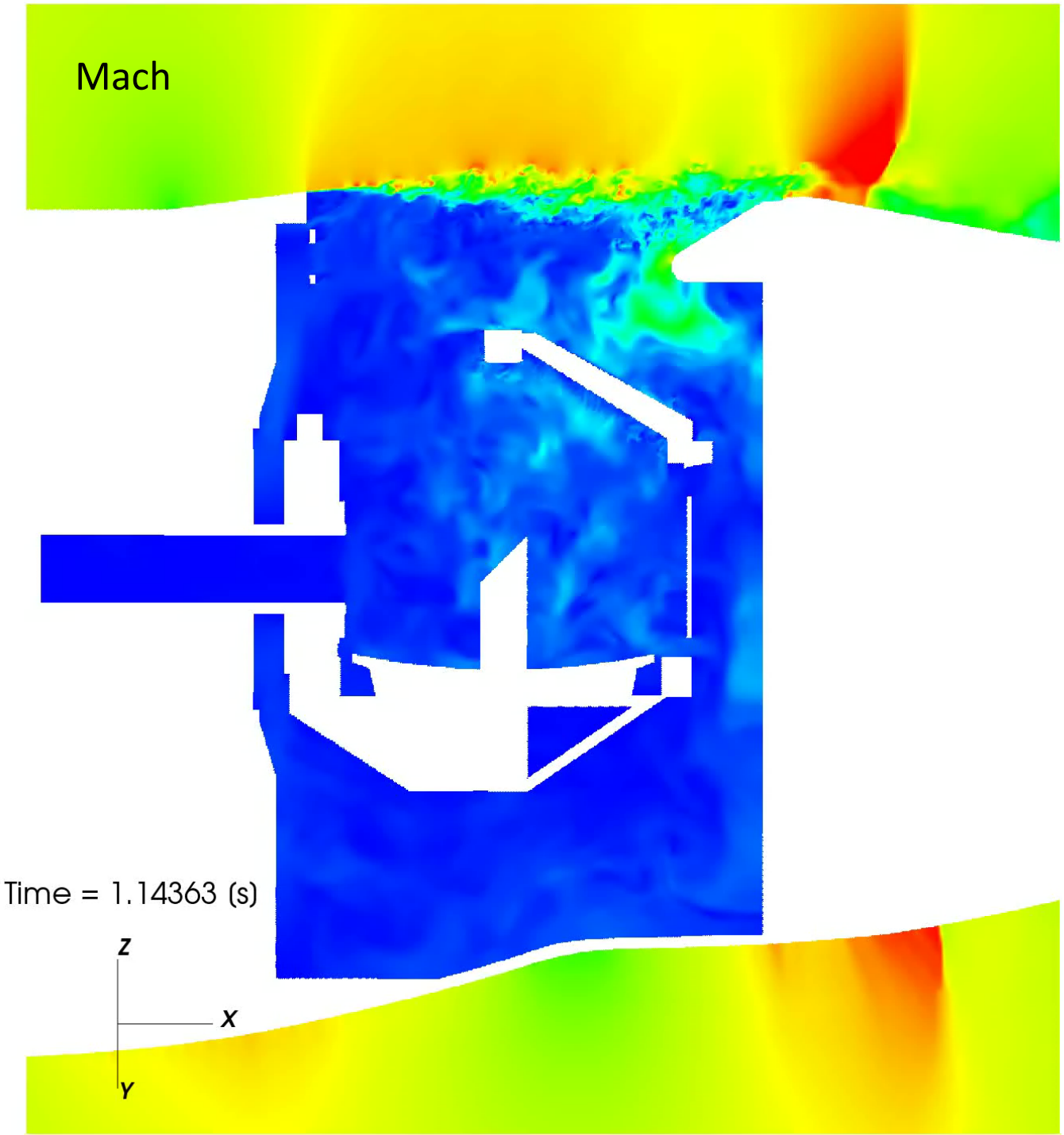

Mean Flow

Generally mean flow field is very similar for both grids. Shear layer affected by enhanced resolution.

Coarse Grid A-B Plane

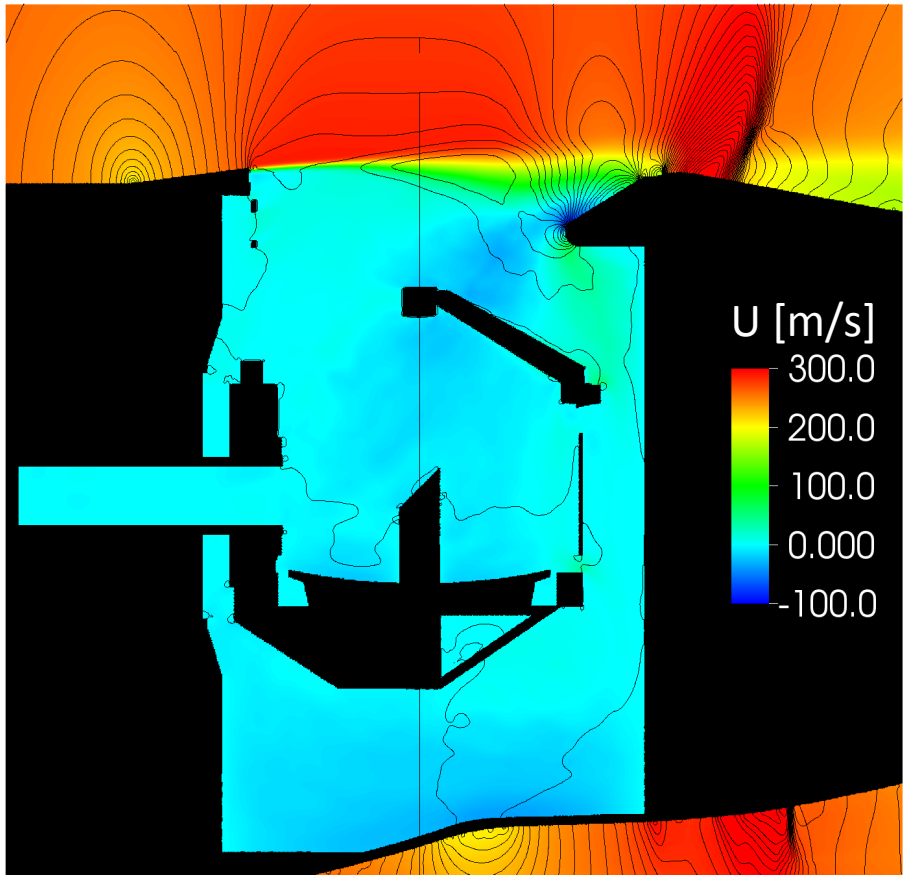

Fine Grid A-B Plane

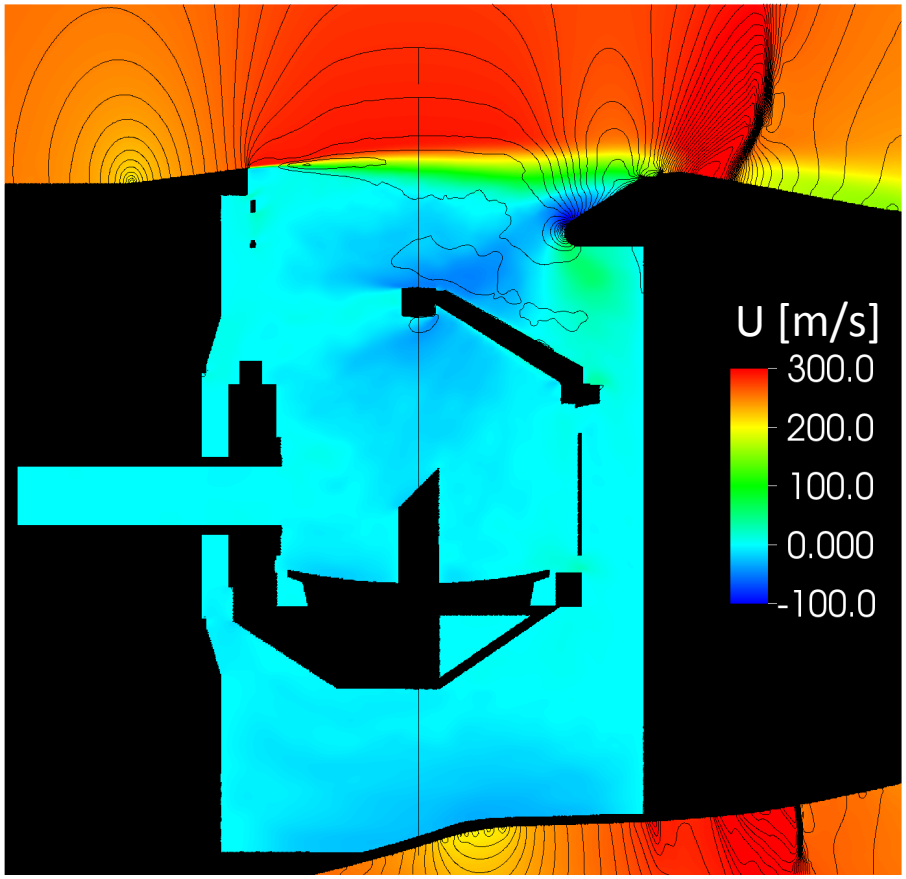

Streamwise velocity (colors) and pressure contour lines

Spectral Analysis:
Frequency at Peak Amplitude [Hz]

Coarse Grid

A-B Plane

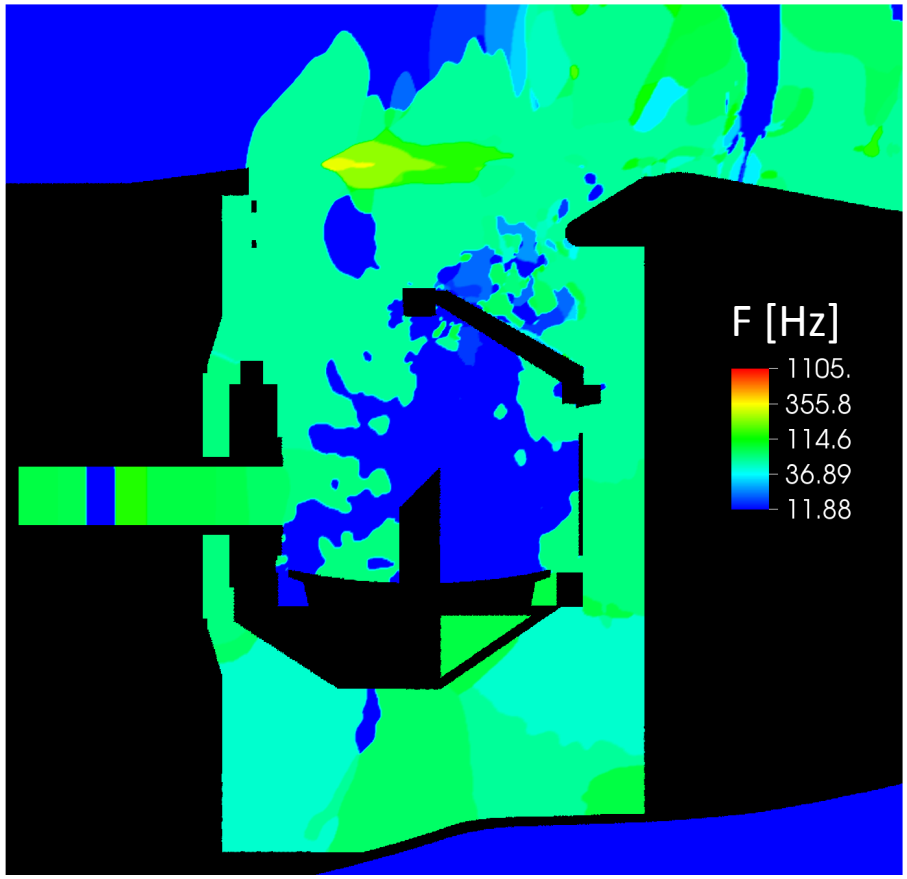

Fine Grid

A-B Plane

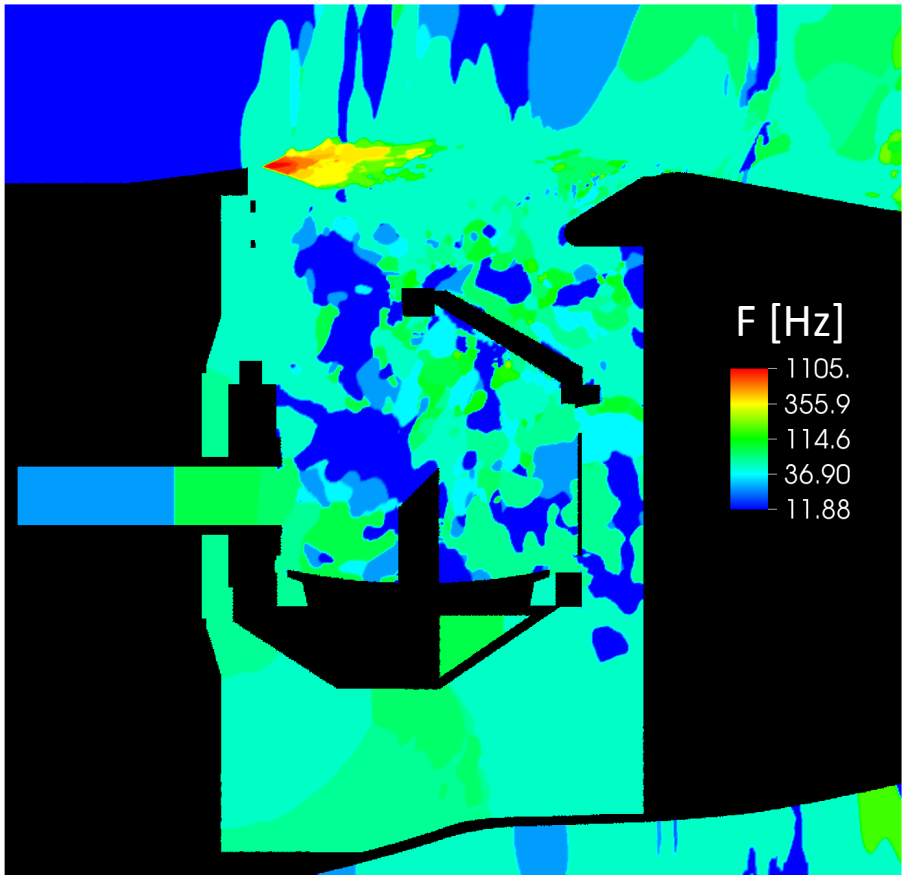

The fine mesh is able to better resolve the initial growth of the shear layer instability.
Highest frequency at the start of the shear layer is associated to primary instability.

Spectral Analysis: Total PSD [dB]

Coarse Grid A-B Plane

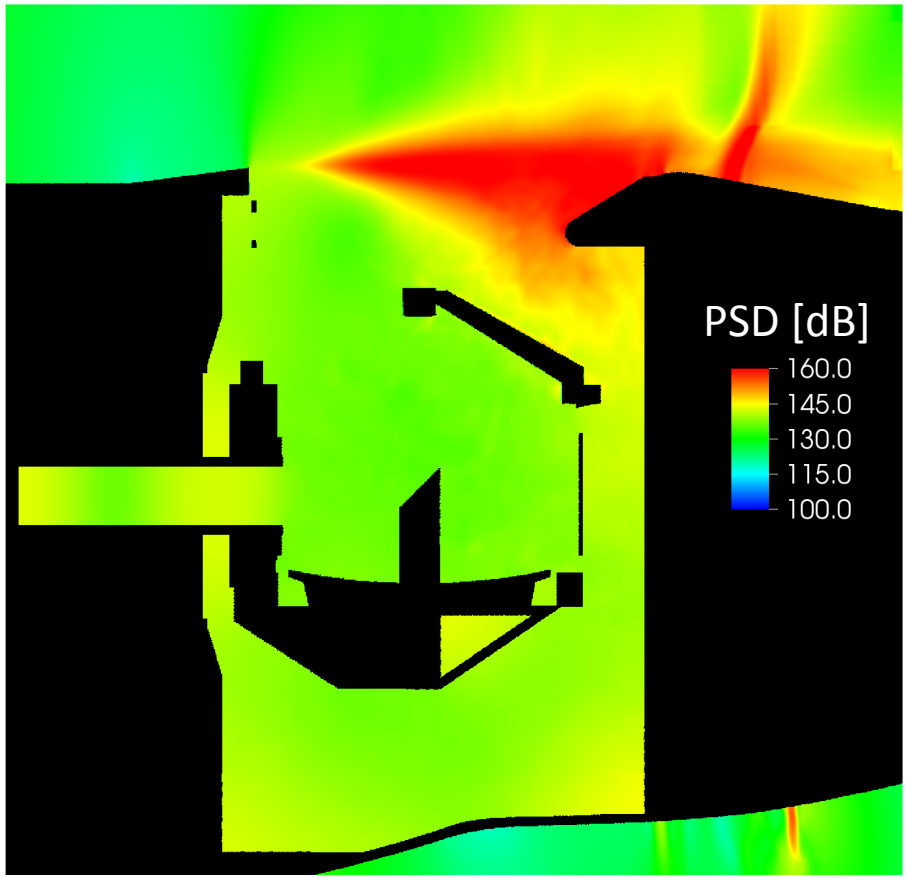

Fine Grid A-B Plane

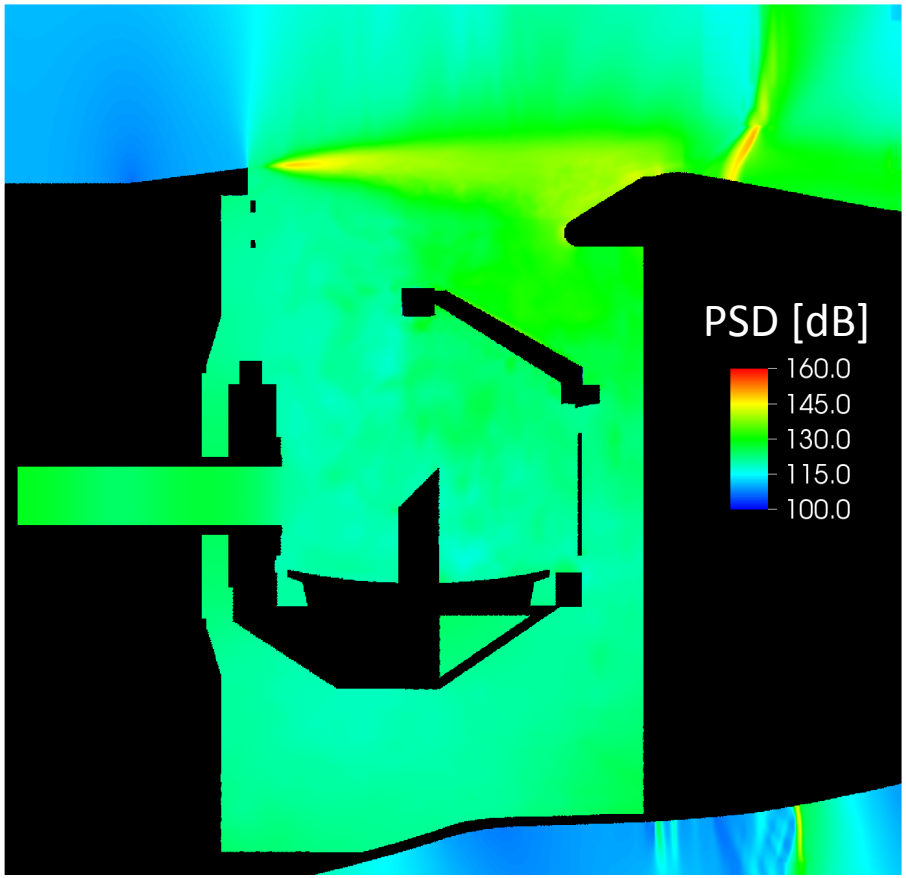

Breakdown of large coherent structures on fine mesh reduces total PSD values. Fine grid solution provides an improved mechanism for the energy cascade.

Disturbance Flow Field:

$$p'(t,x) = p(t,x) - \overline{p}(x)$$

$$u'(t,x) = u(t,x) - \overline{u}(x)$$

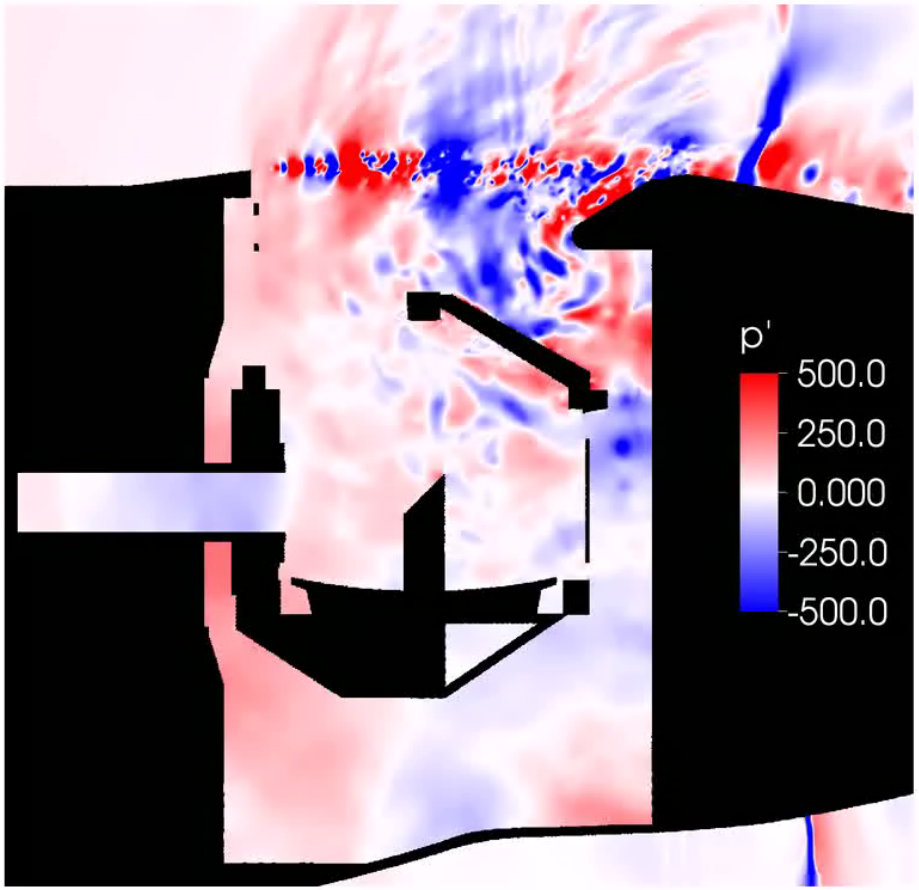

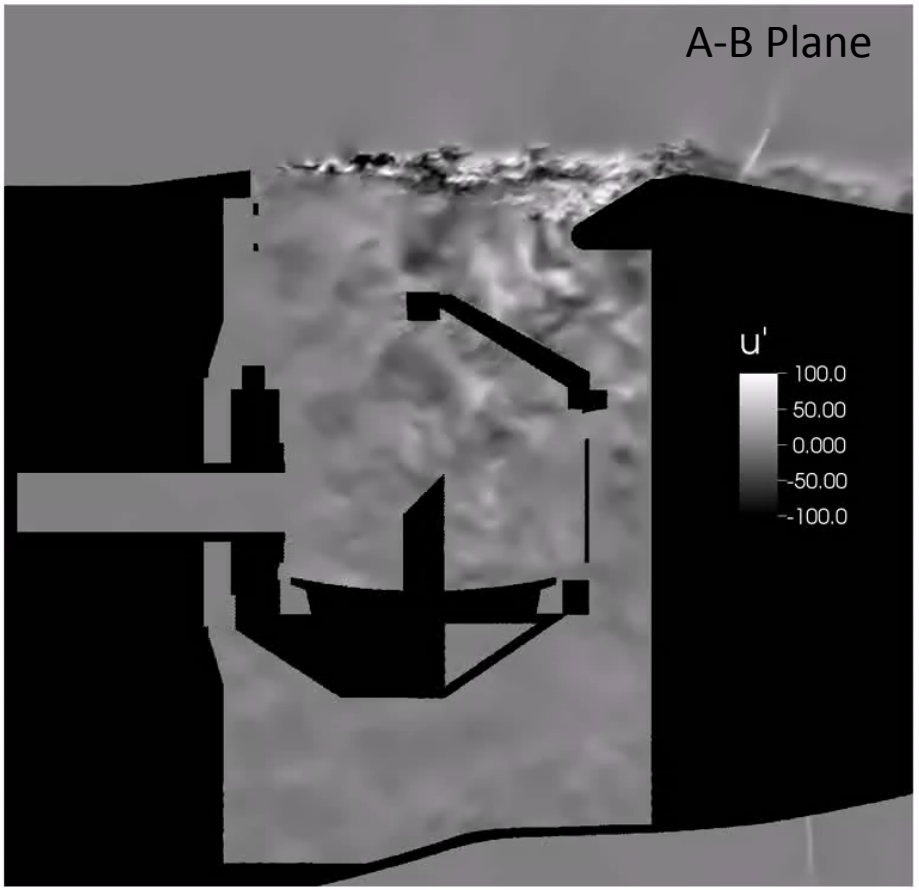

- Acoustic radiation away from shear layer
- Unsteady pressure field inside cavity
- Interacting pressure field and shock

- Small scale velocity fluctuations
- Impingement of shear layer on vehicle
- Momentum transfer into cavity

Instantaneous |Grad(Density)|

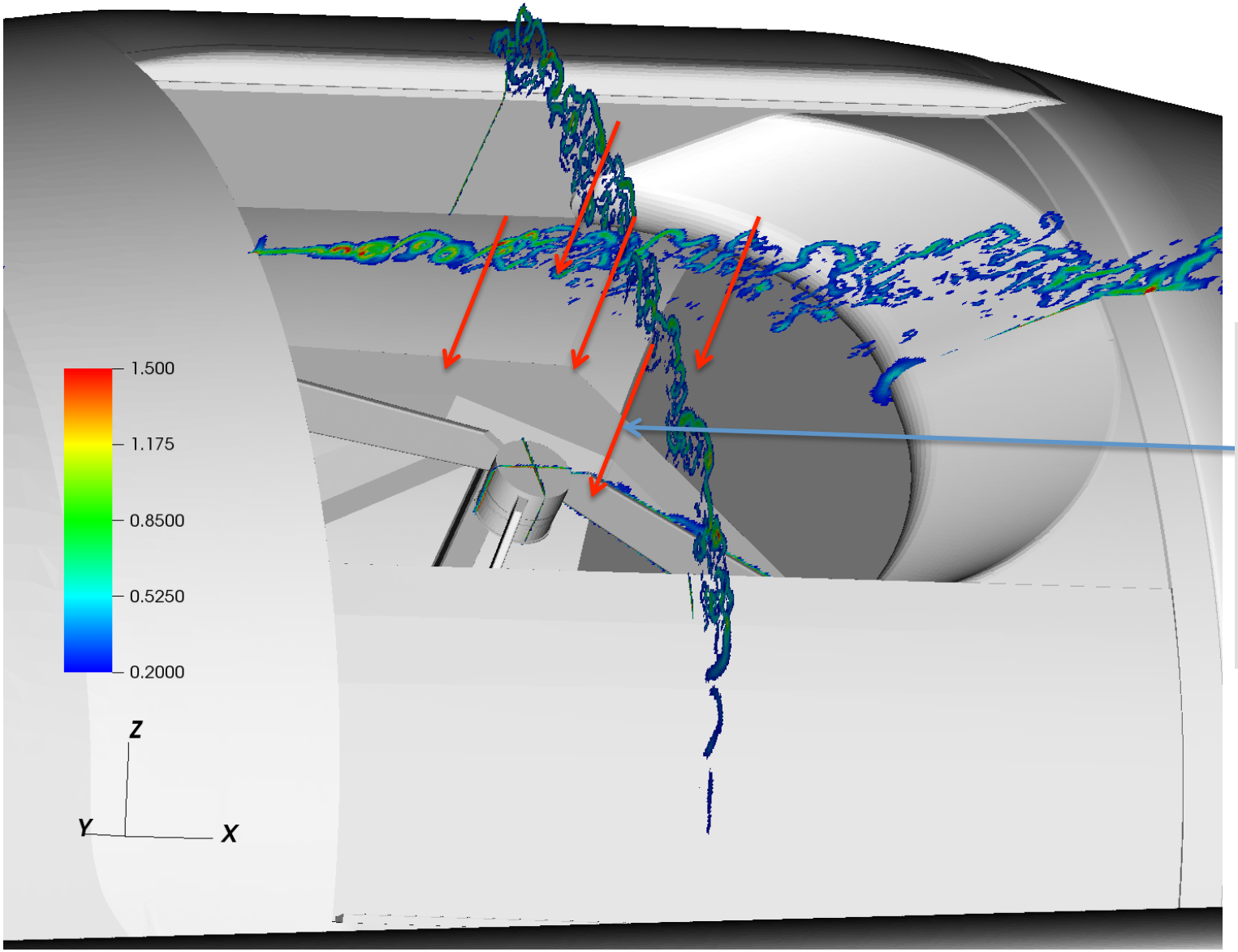

Telescope line-of-sight (indicated by red arrows) crosses significant density gradients (i.e. variations in refractive index)

Outline

- Background/Motivation
- LAVA Solver
- SOFIA Simulation Setup
- General Flow Features
- Spectral Analysis
- Proper Orthogonal Decomposition Analysis
- Conclusions

Cutting planes and mesh

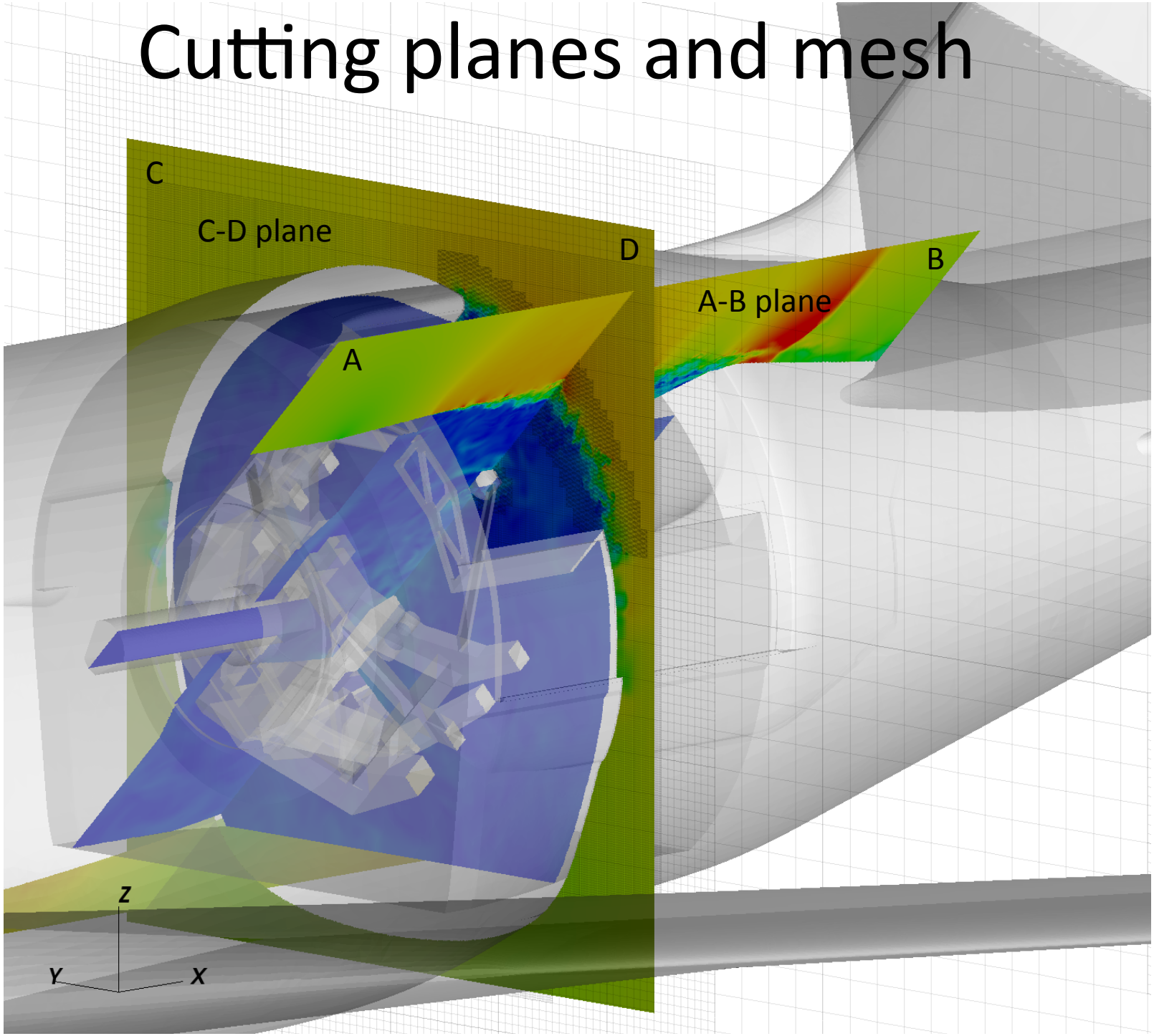

Spectral Analysis:
Frequency at Peak Amplitude [Hz]

A-B Plane

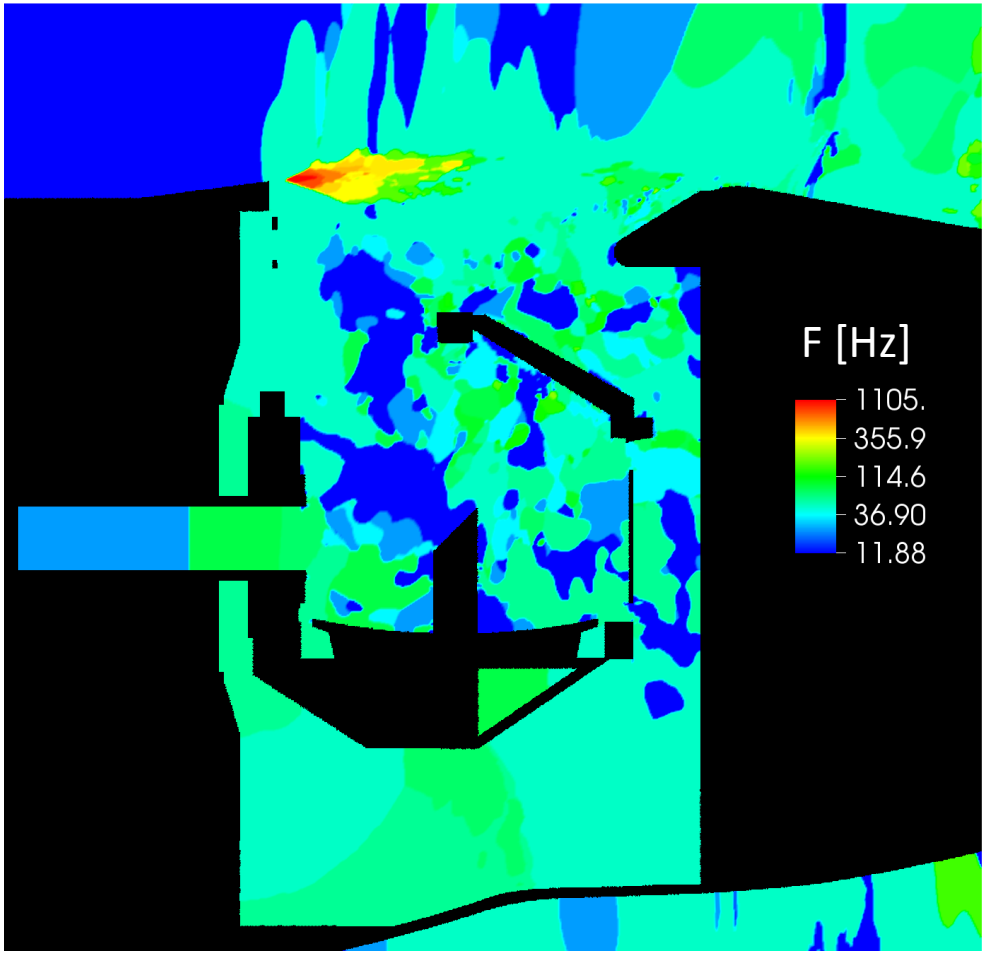

C-D Plane

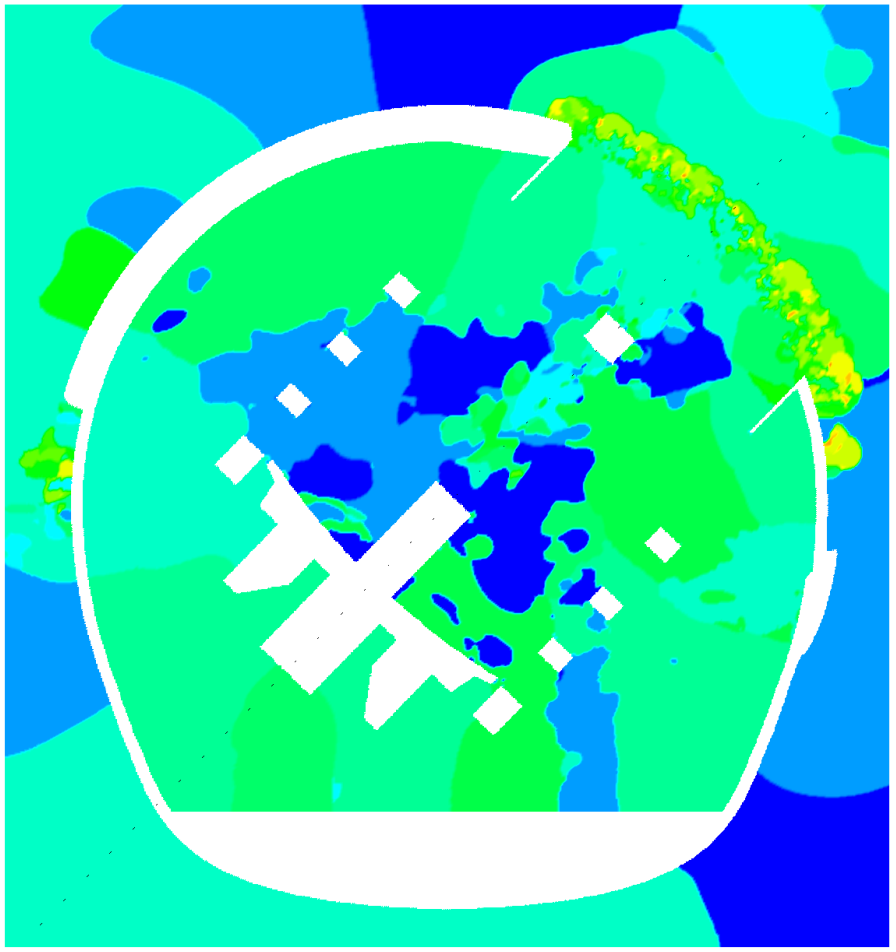

High frequencies at shear layer inception associated to KH-instability. Nearly uniform low peak frequency observed everywhere inside cavity.

Spectral Analysis: Peak Amplitude

(A-B Plane)

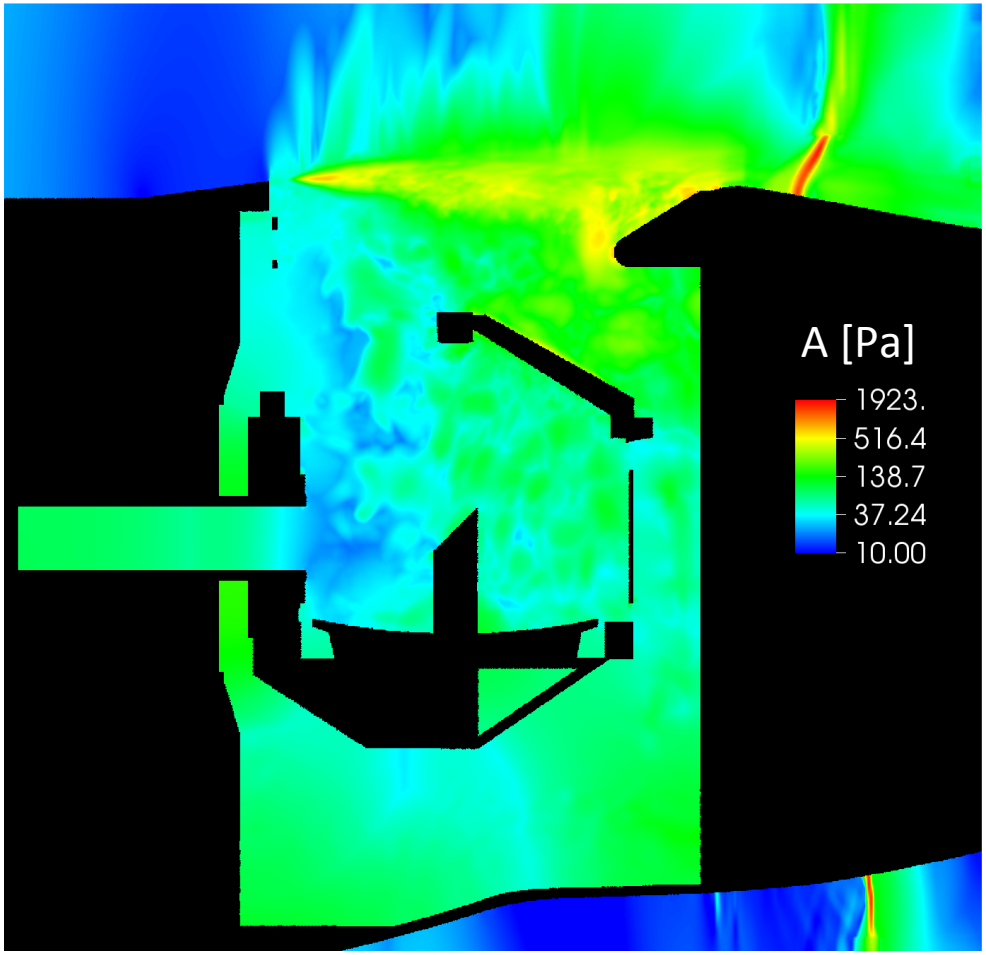

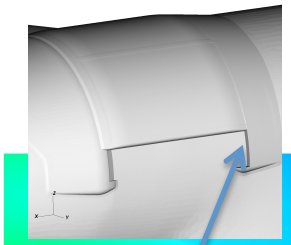

(C-D Plane)

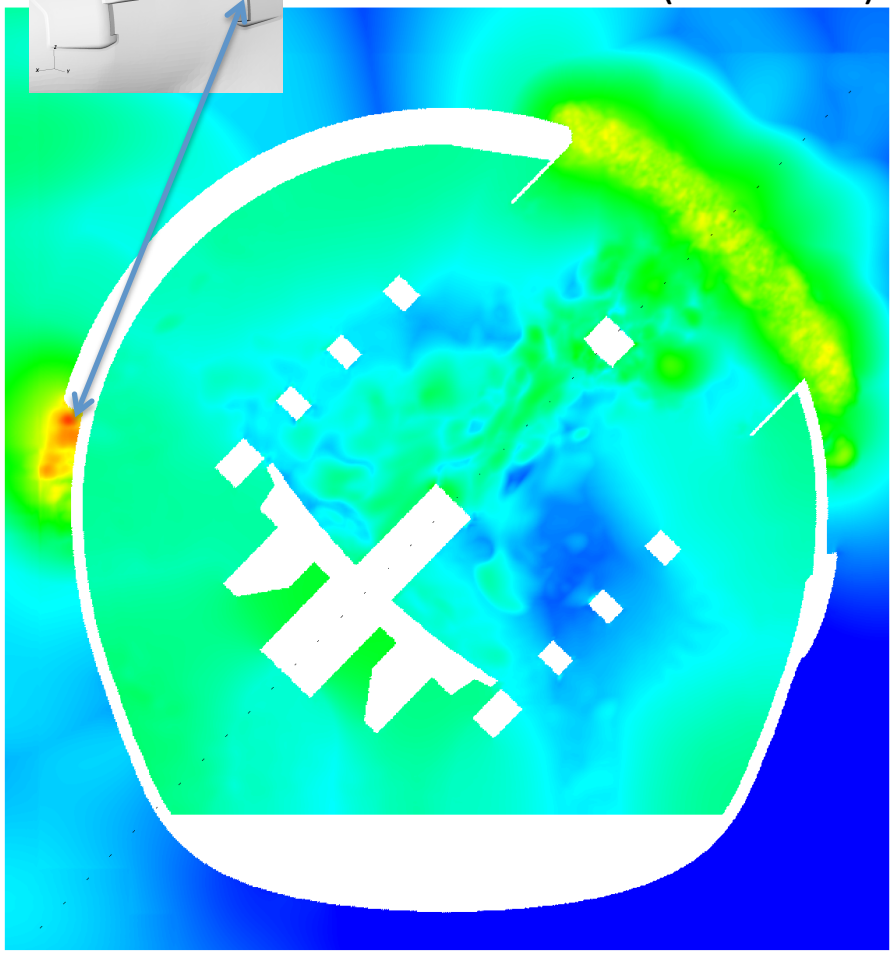

Highest peak amplitude at shocks and in shear layer region. Moderate peak amplitude in cavity. Further analysis elaborates on particular frequency characteristics, i.e., broad vs. narrow band.

Spectral Analysis: Total PSD [dB]

A-B Plane

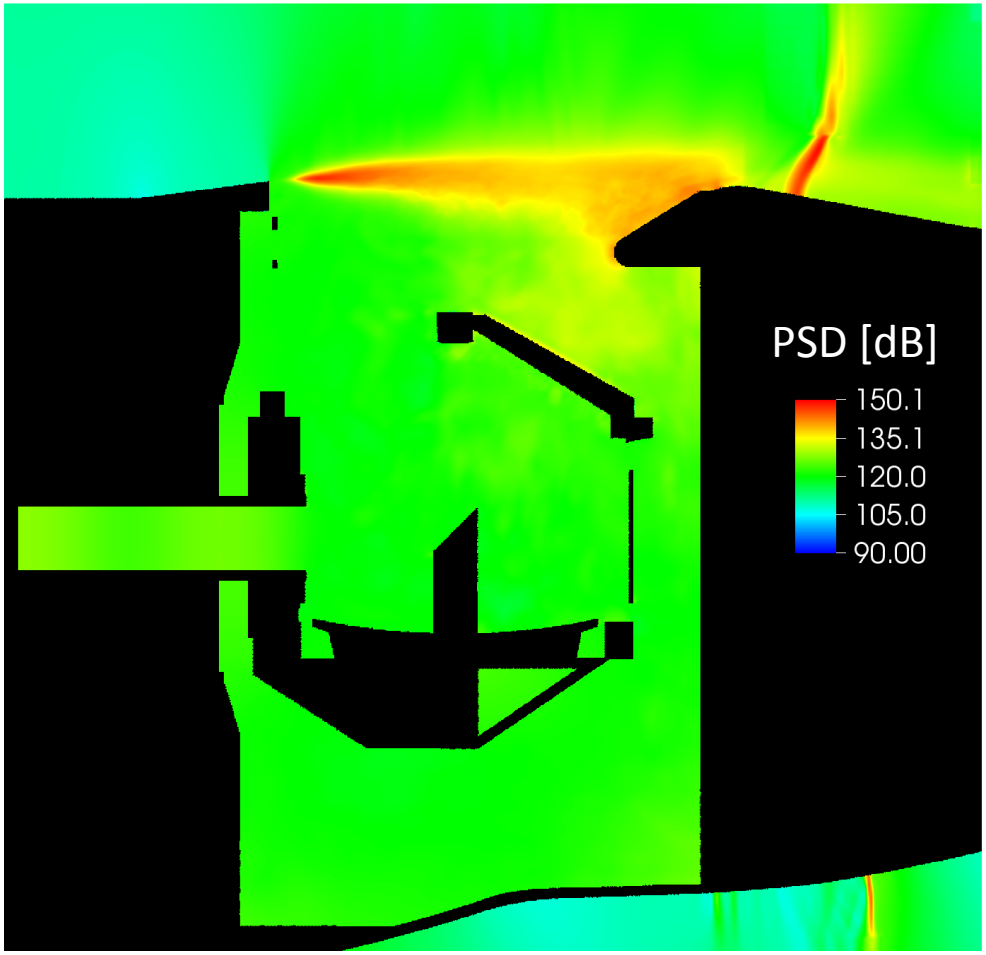

C-D Plane

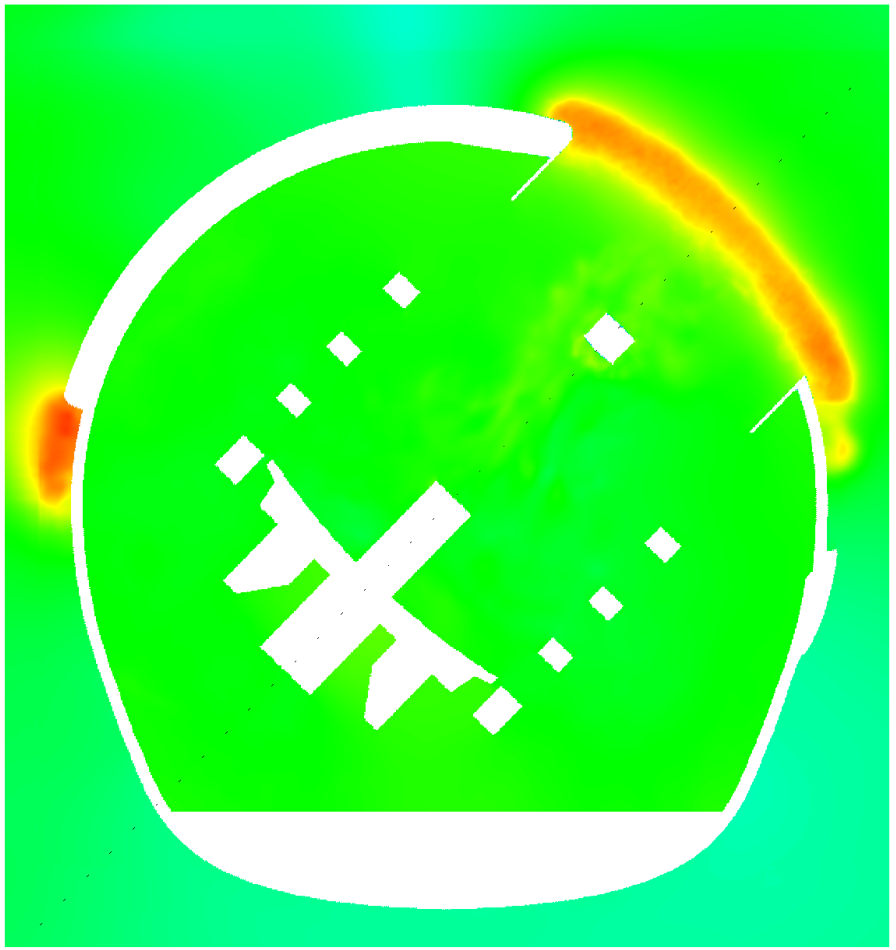

Total PSD provides information about noise level and was compared to **observations during flight inside the cavity were at the ~120dB level**.

Spectral Analysis: Point Probe Locations

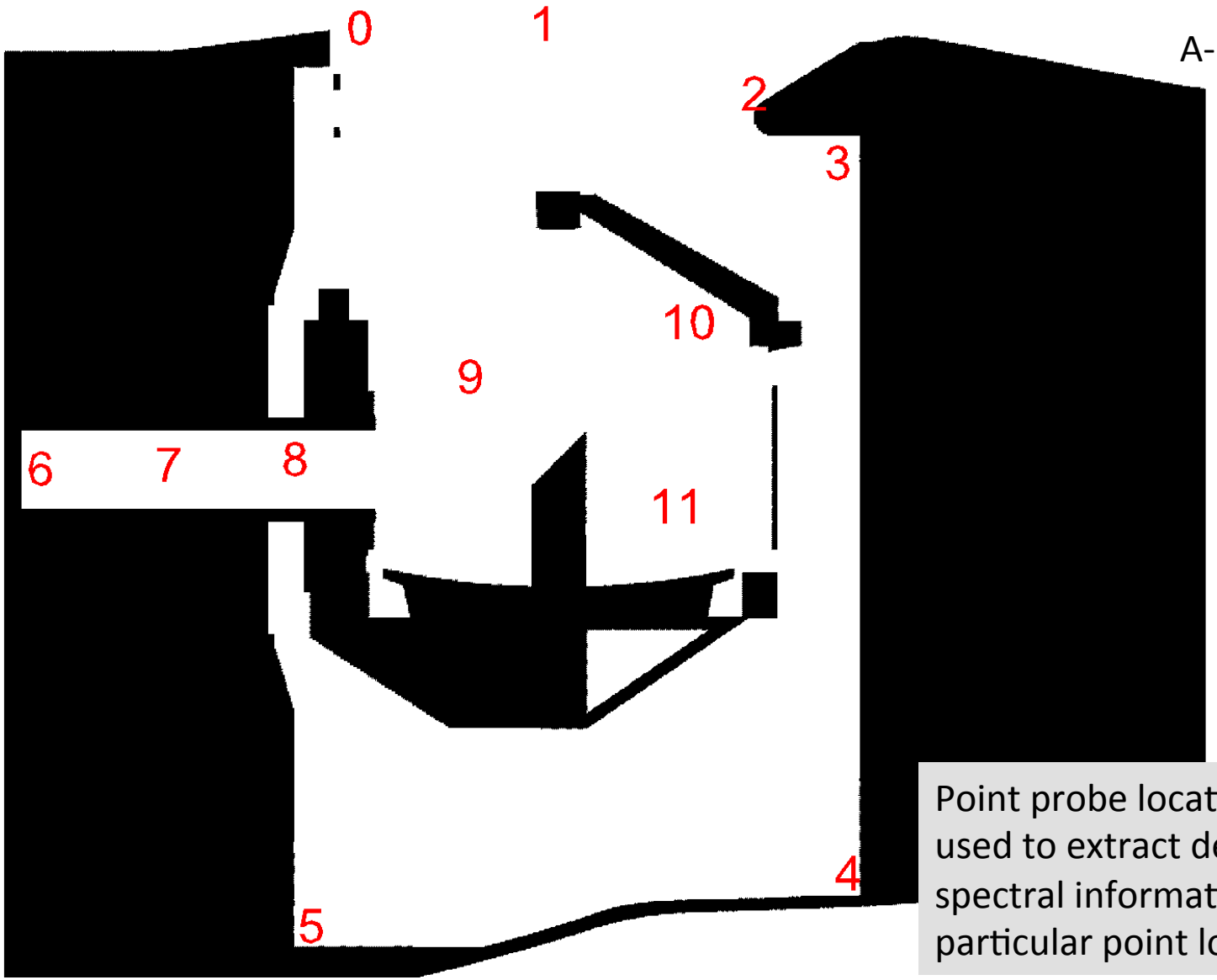

Point probe locations used to extract detailed spectral information at particular point locations.

Velocity Power Spectra

Streamwise (u')

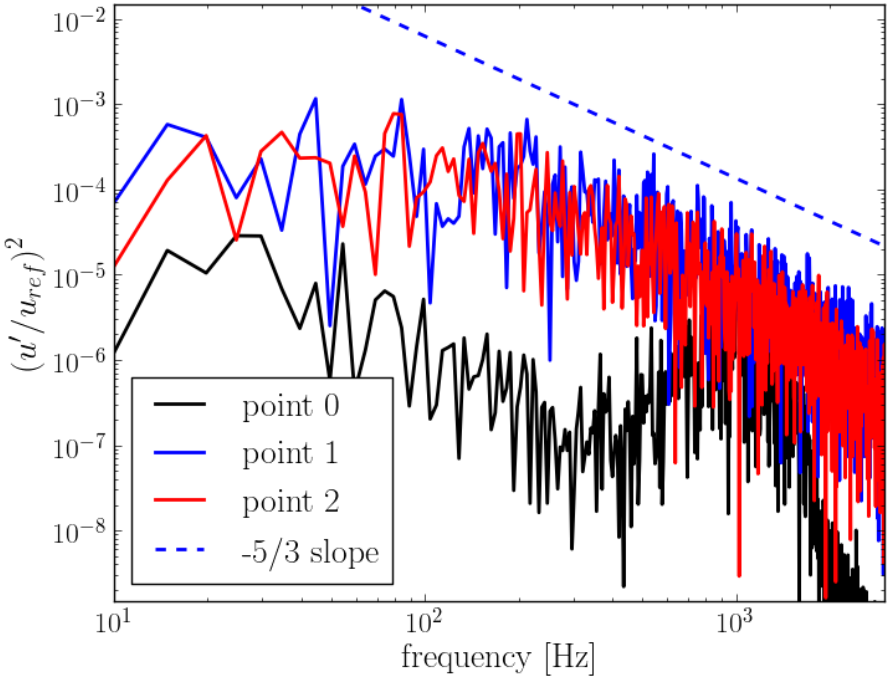

"Spanwise" (v')

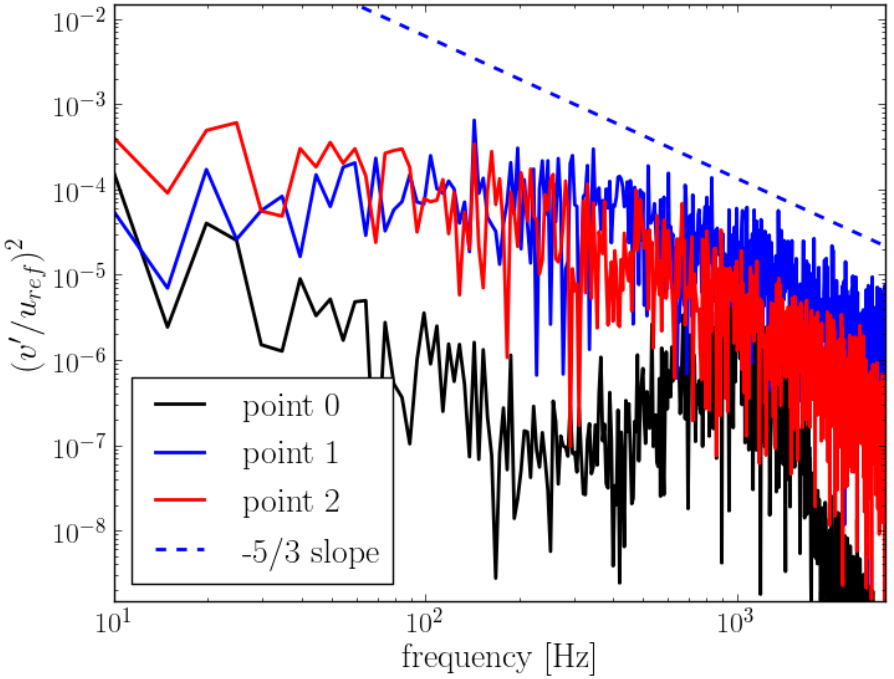

Point Locations

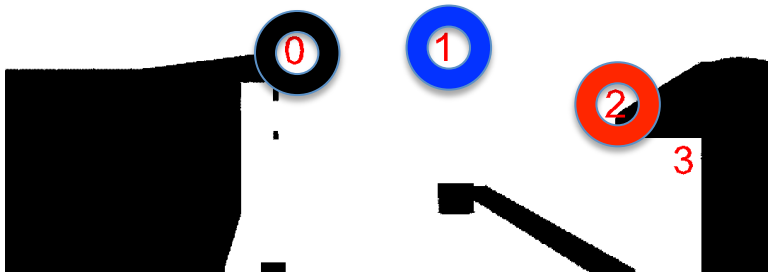

Power spectra at point 0 displays high frequency band related to shear layer instability (~1000Hz). Further downstream broadening of spectrum and increase in amplitude. Theoretical sub-inertial scaling law indicated. Further analysis of turbulent statistics may provide further insight.

Spectral Analysis: Probes

Pressure field displays frequency peak at shear layer surface impingement (point 2) in 50-60 Hz range.

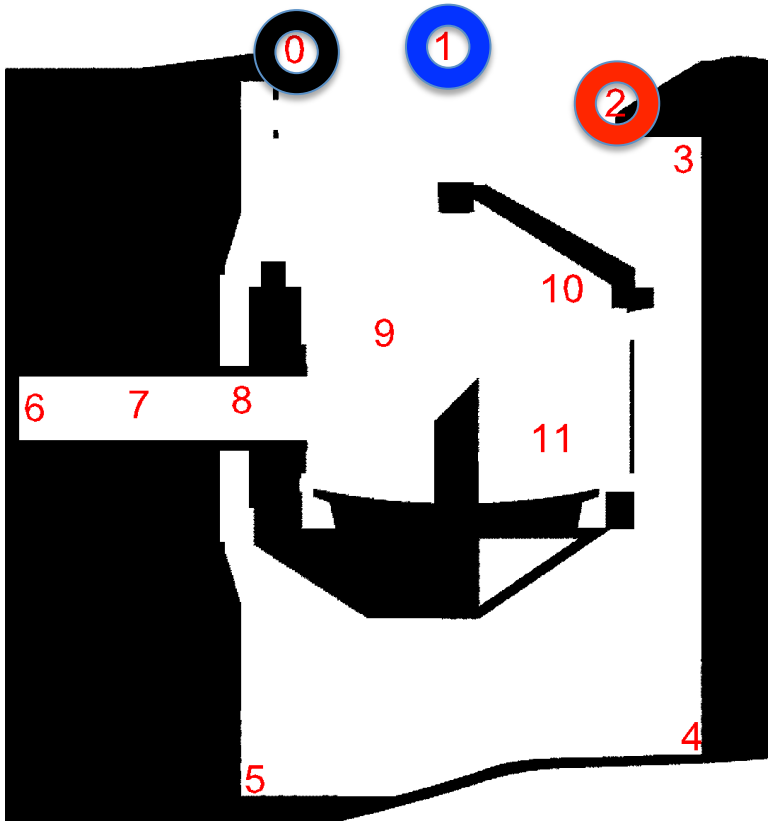

A-B Plane

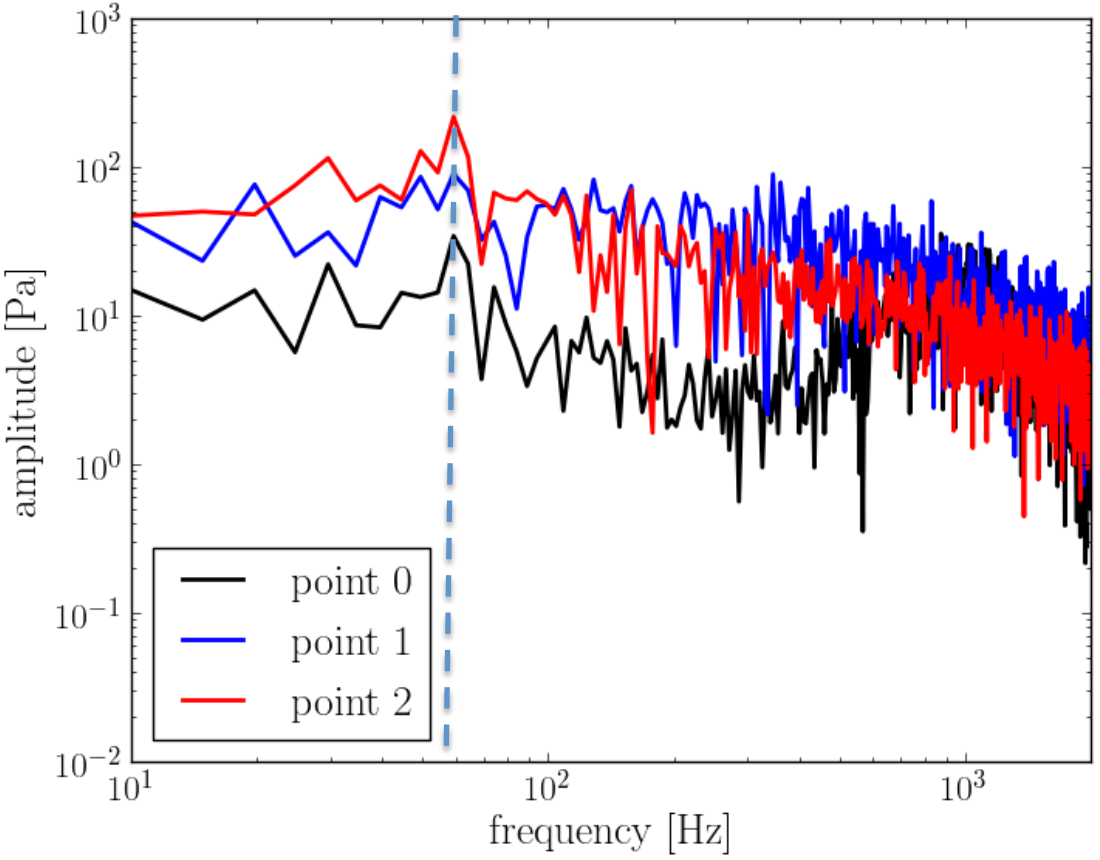

Spectral Analysis: Probes

Frequency peak at point 2 can also be observed at points 10 and 11.
Broadband noise level associated with highly unsteady shear layer.

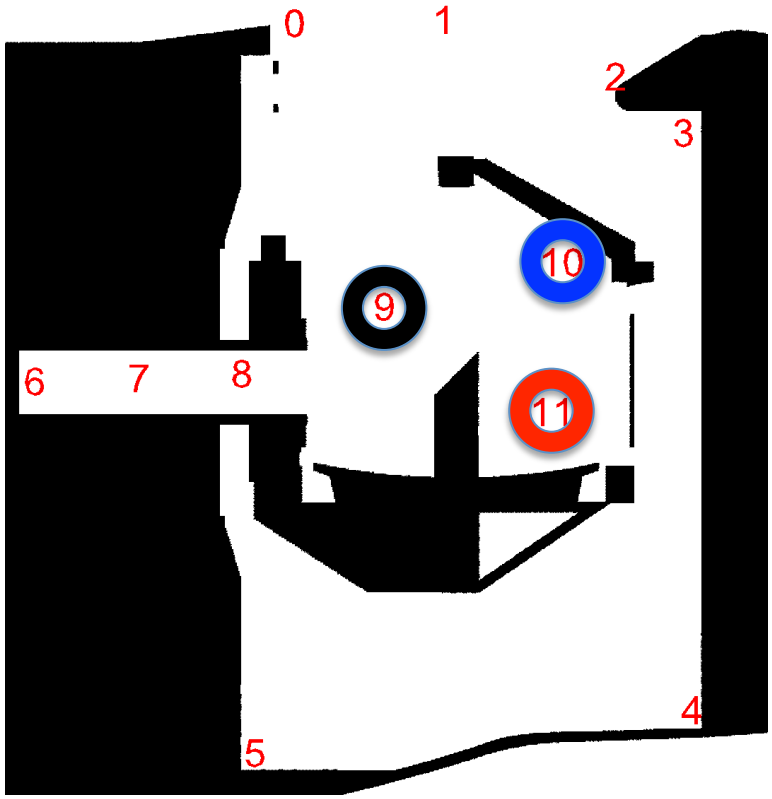

A-B Plane

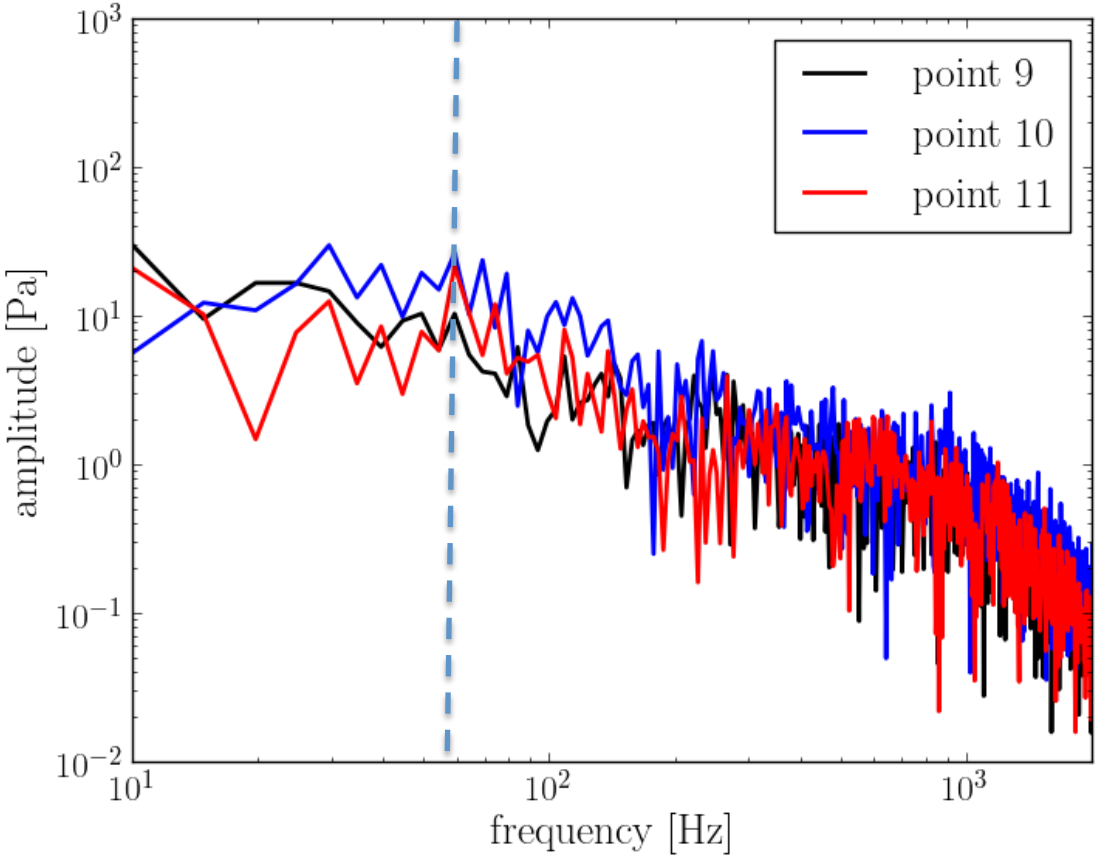

Spectral Analysis: Probes

Corner points display elevated amplitudes in frequency range 20-100Hz. Increased broadband noise at point 3 associated with shear layer proximity.

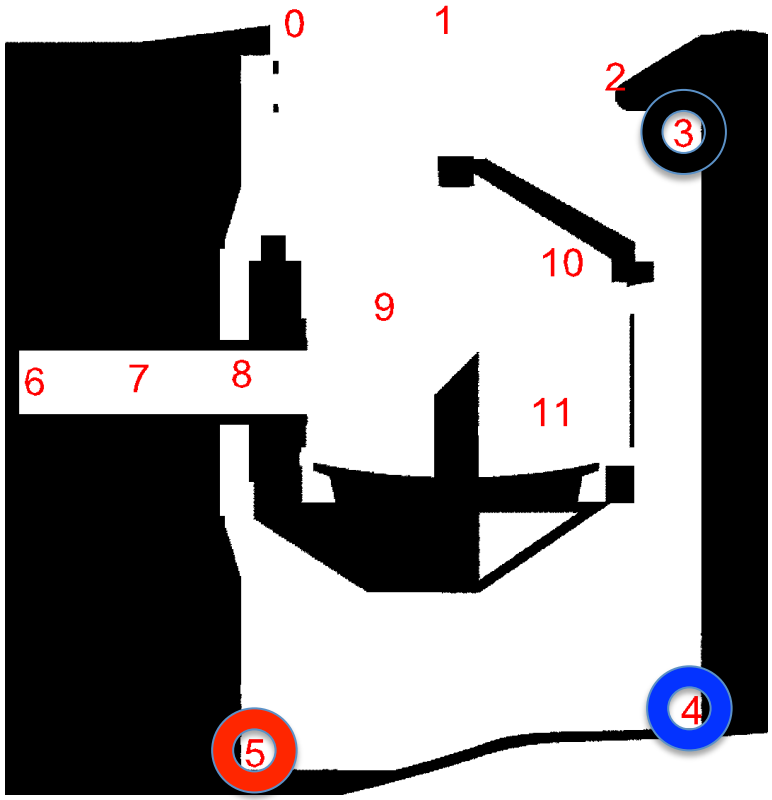

A-B Plane

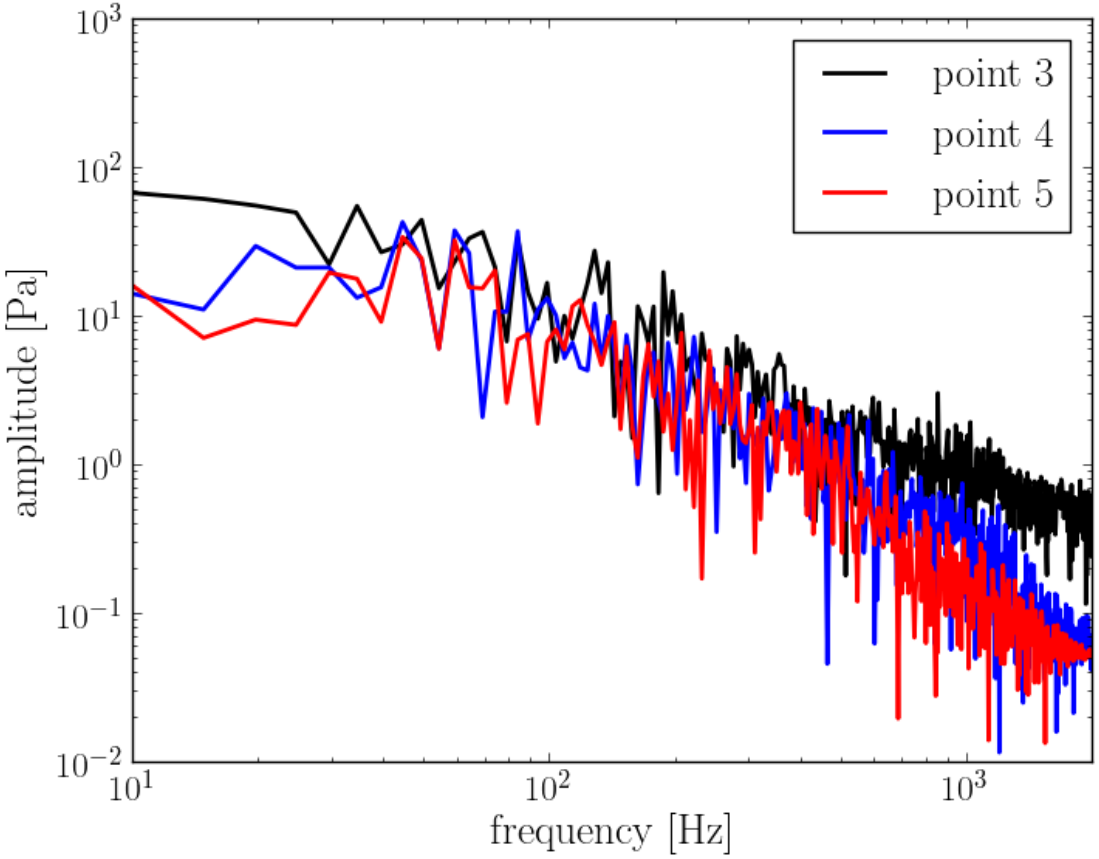

Spectral Analysis: Probes

Low frequency peaks (25 and 78Hz) at points 6-8 are related to standing waves inside observation tube.

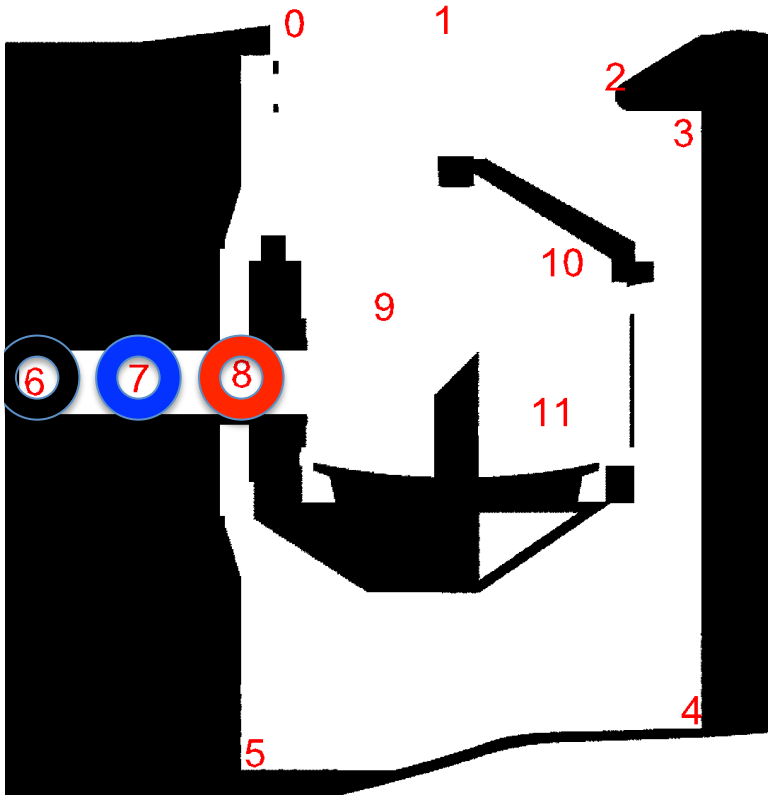

A-B Plane

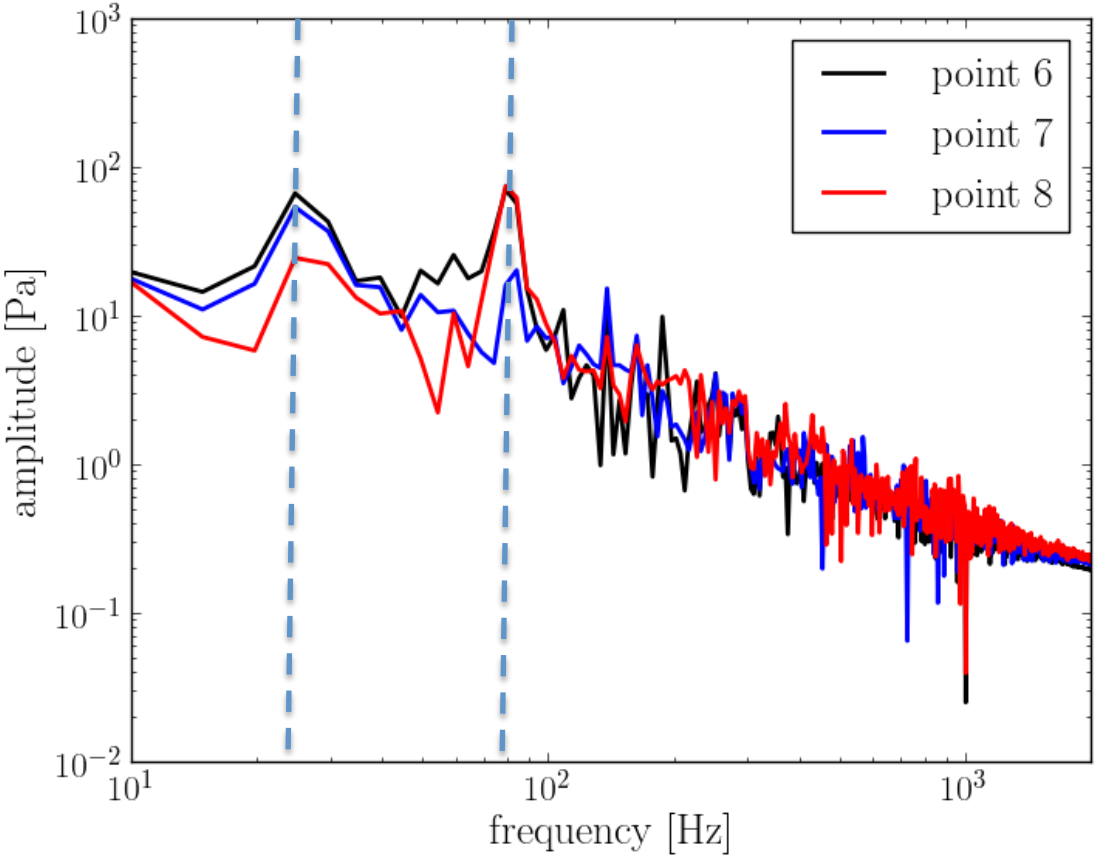

Spectral Analysis at 19.6 Hz

Amplitude [Pa]

Phase

A-B Plane

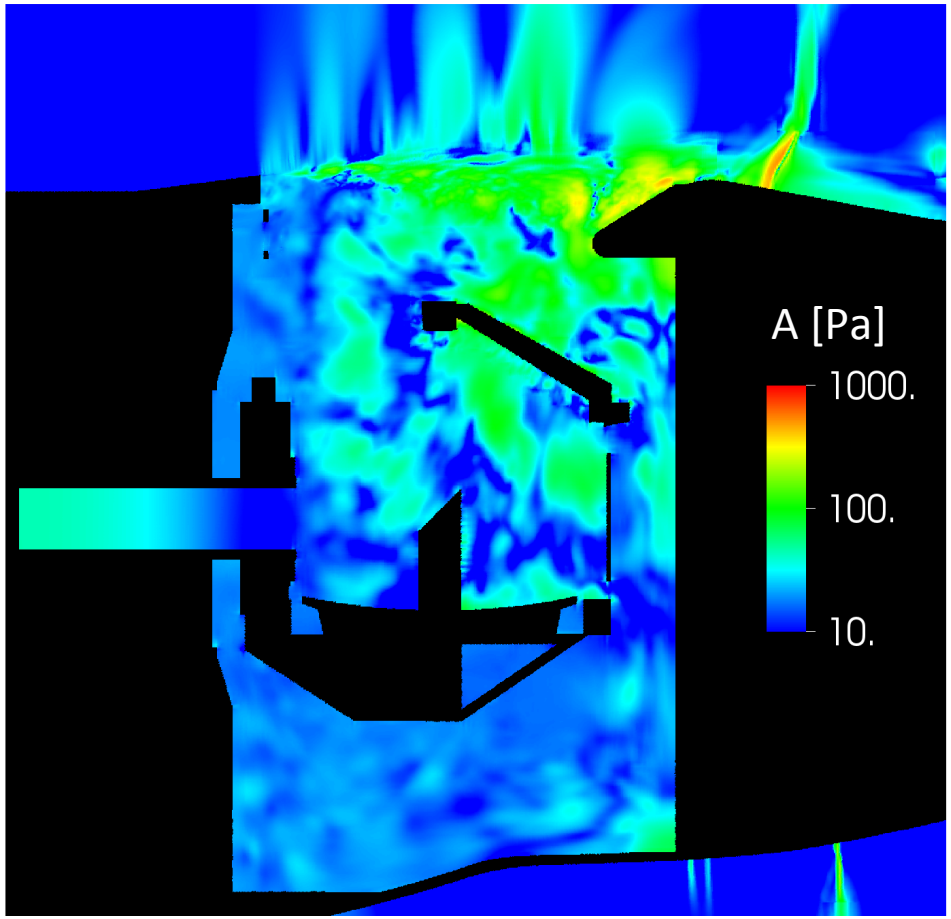

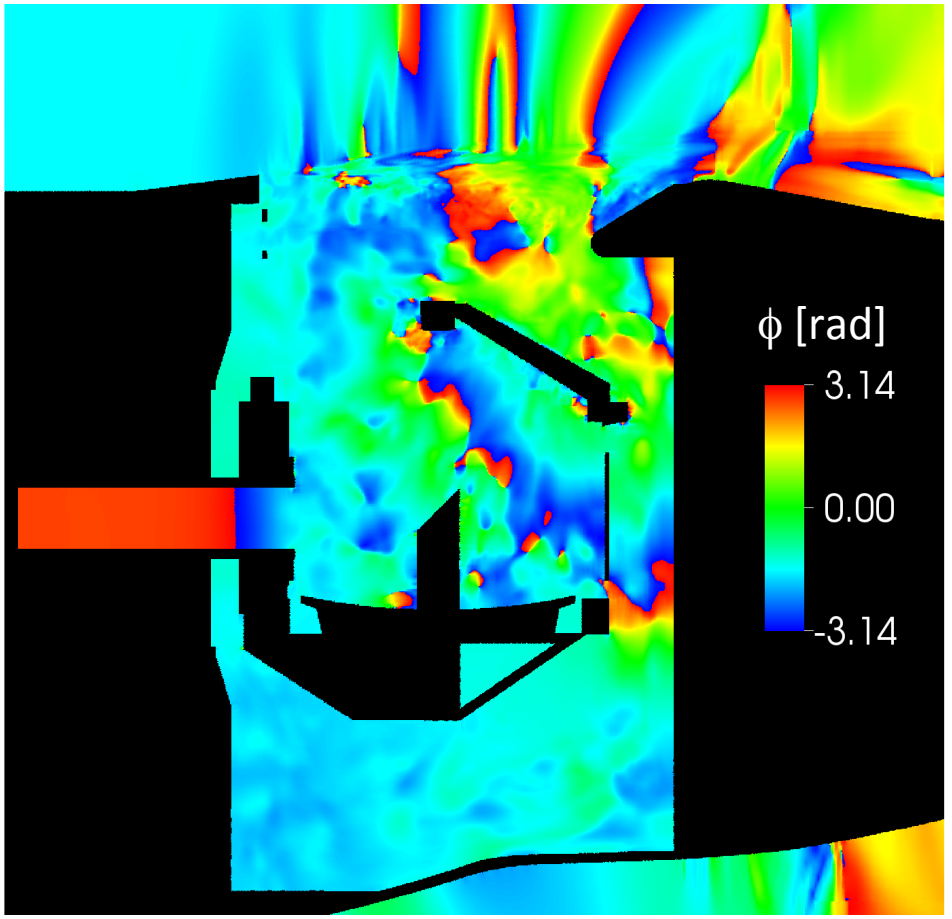

Low frequency mode with phase $\phi=\pi$ is dominant inside observation tube.
No real wave patterns can be observed in phase plot due to large wavelength.

Spectral Analysis at 24.5 Hz

Amplitude [Pa]

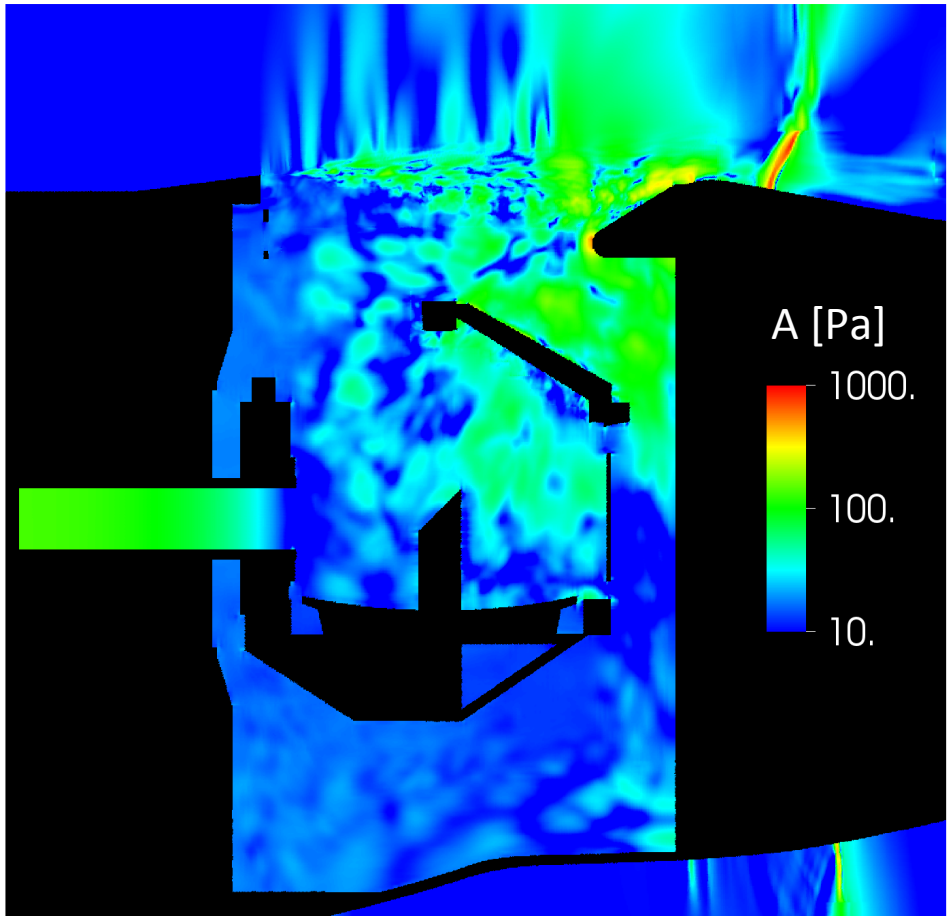

Phase

A-B Plane

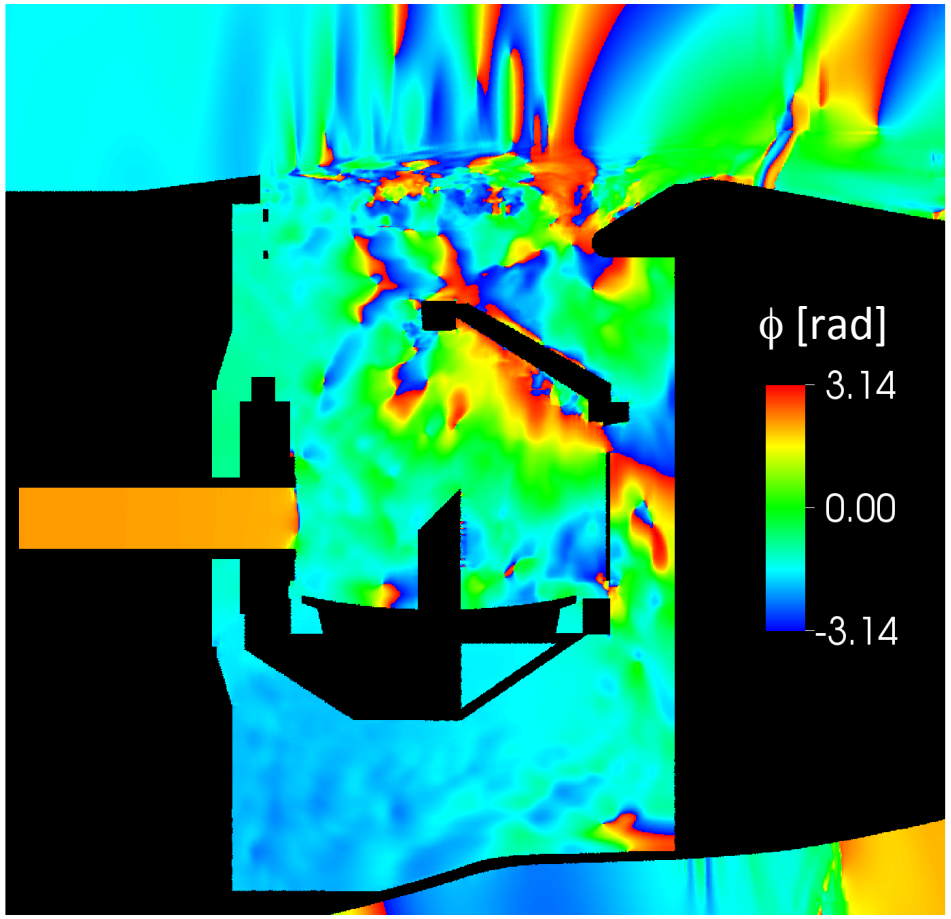

Similar observations as previous slide.
Frequency seems tuned to length of observation tube.

Spectral Analysis at 44.1 Hz

Amplitude [Pa]

Phase

A-B Plane

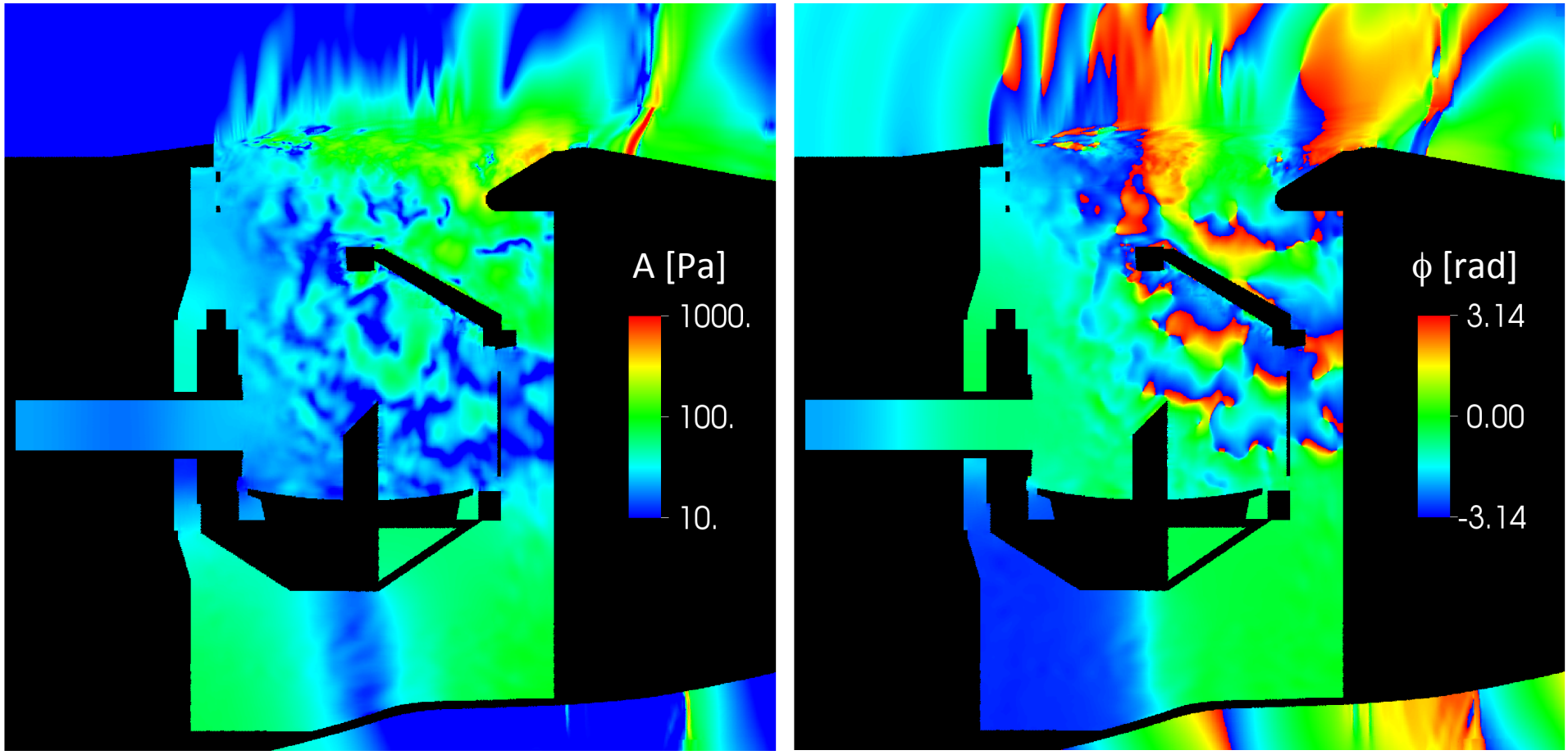

Cavity mode: high amplitudes and phase shift from left to right below telescope. Pressure wave radiation away from impingement region. Could induce structural vibrations.

Spectral Analysis at 58.4 Hz

Amplitude [Pa]

Phase

A-B Plane

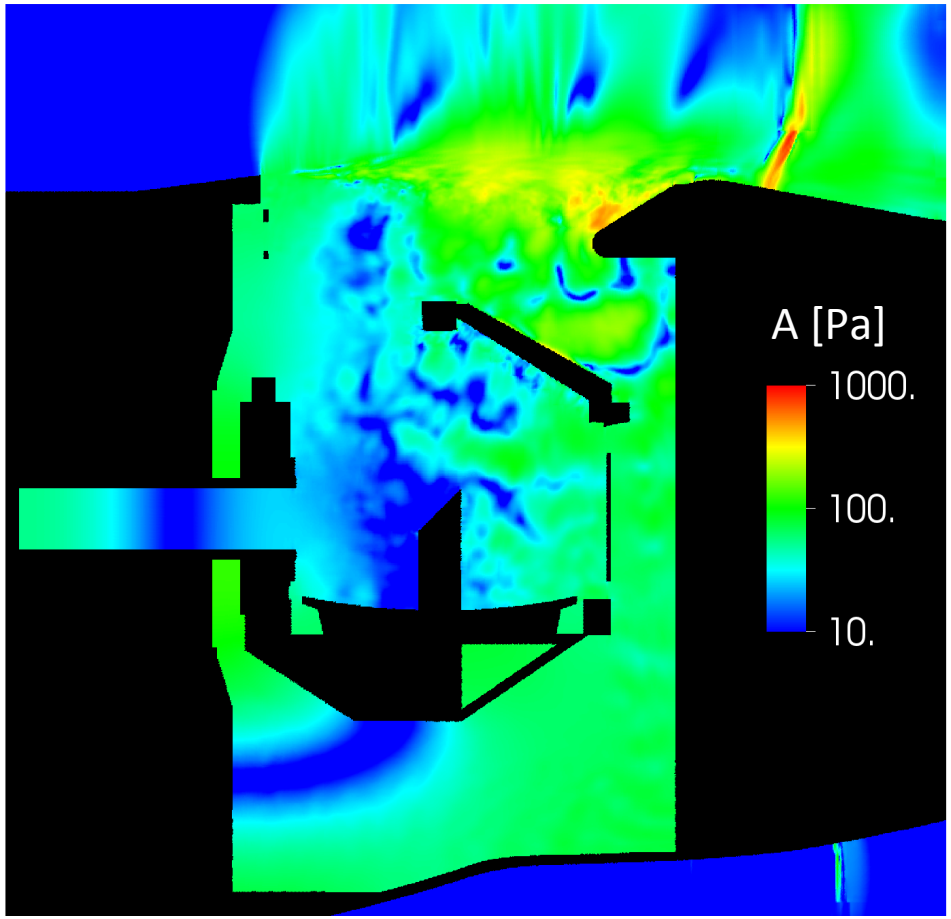

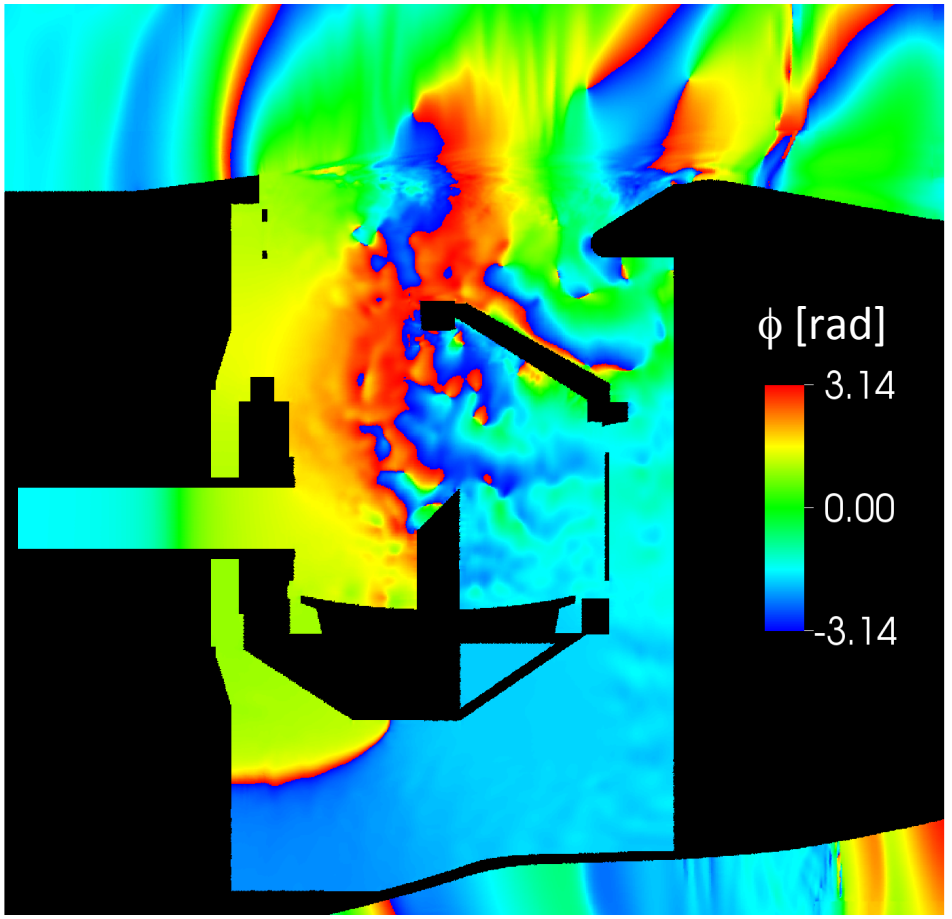

High amplitude inside cavity suggests presence of cavity mode at this frequency.
Mode shape cannot be clearly distinguished from phase plot (cross vehicle coupling possible)

Spectral Analysis at 78.4 Hz

Amplitude [Pa]

Phase

A-B Plane

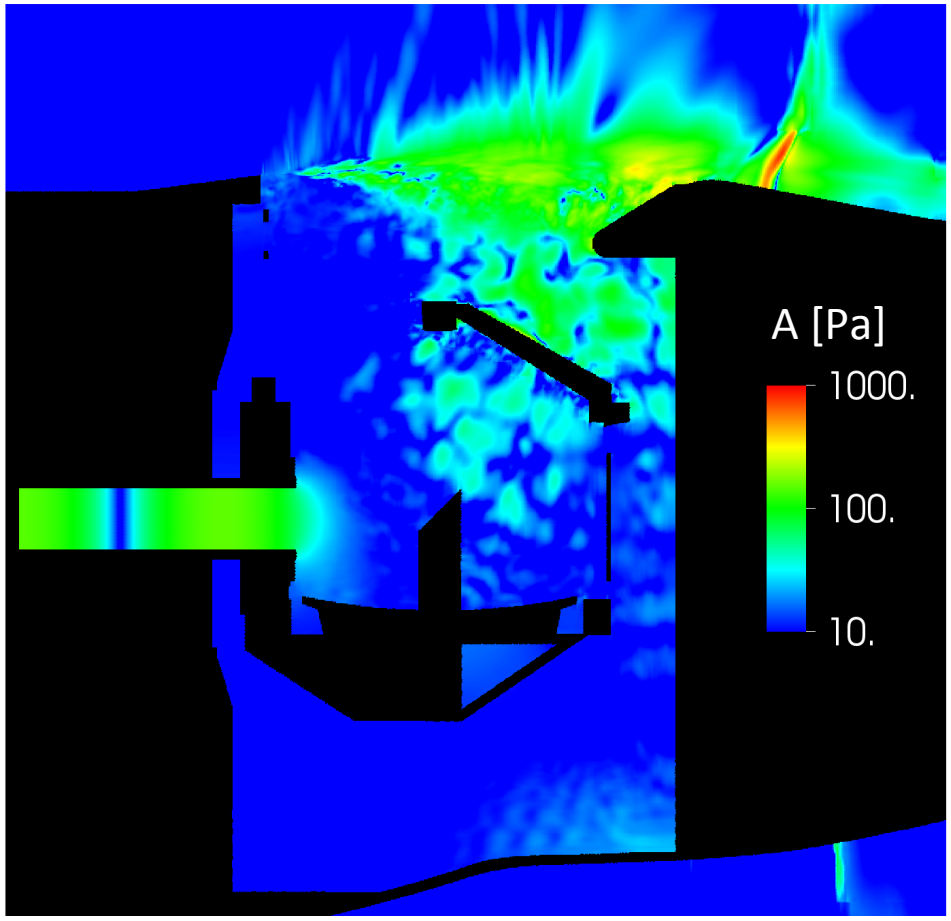

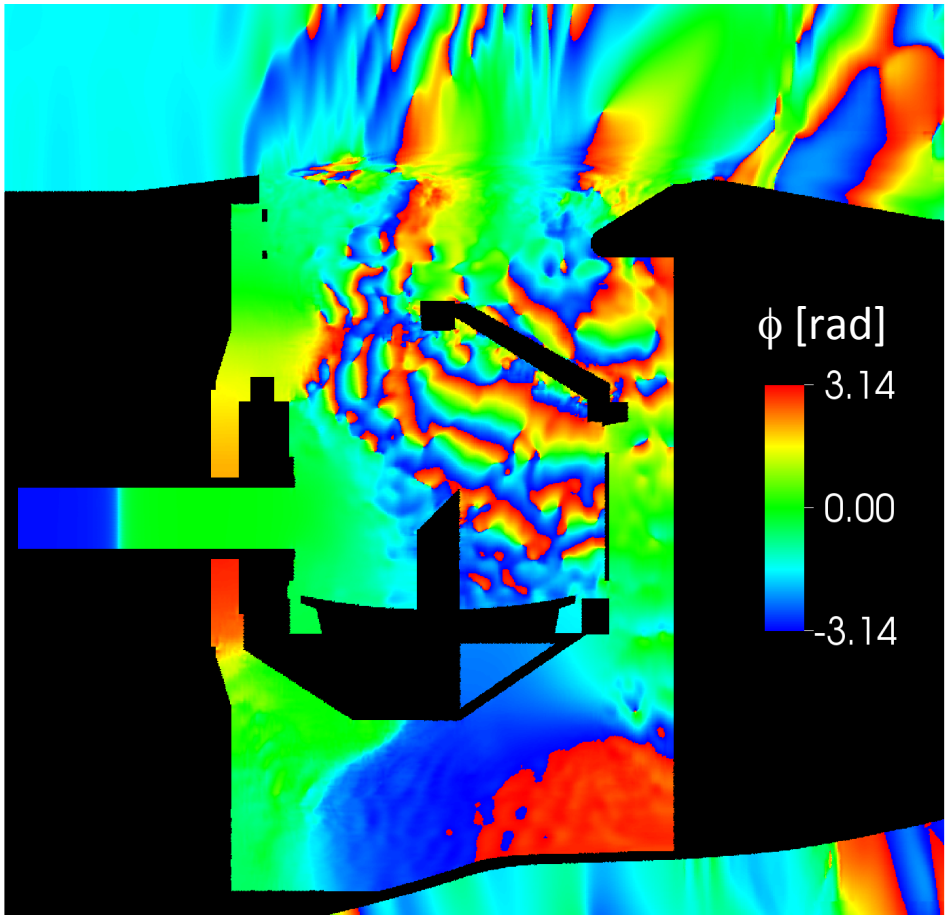

Low amplitudes inside cavity. Phase plot suggests pressure wave propagation from impingement region and/or possible vortex shedding from upper telescope arm.

Spectral Analysis at 342 Hz

Amplitude [Pa]

Phase

A-B Plane

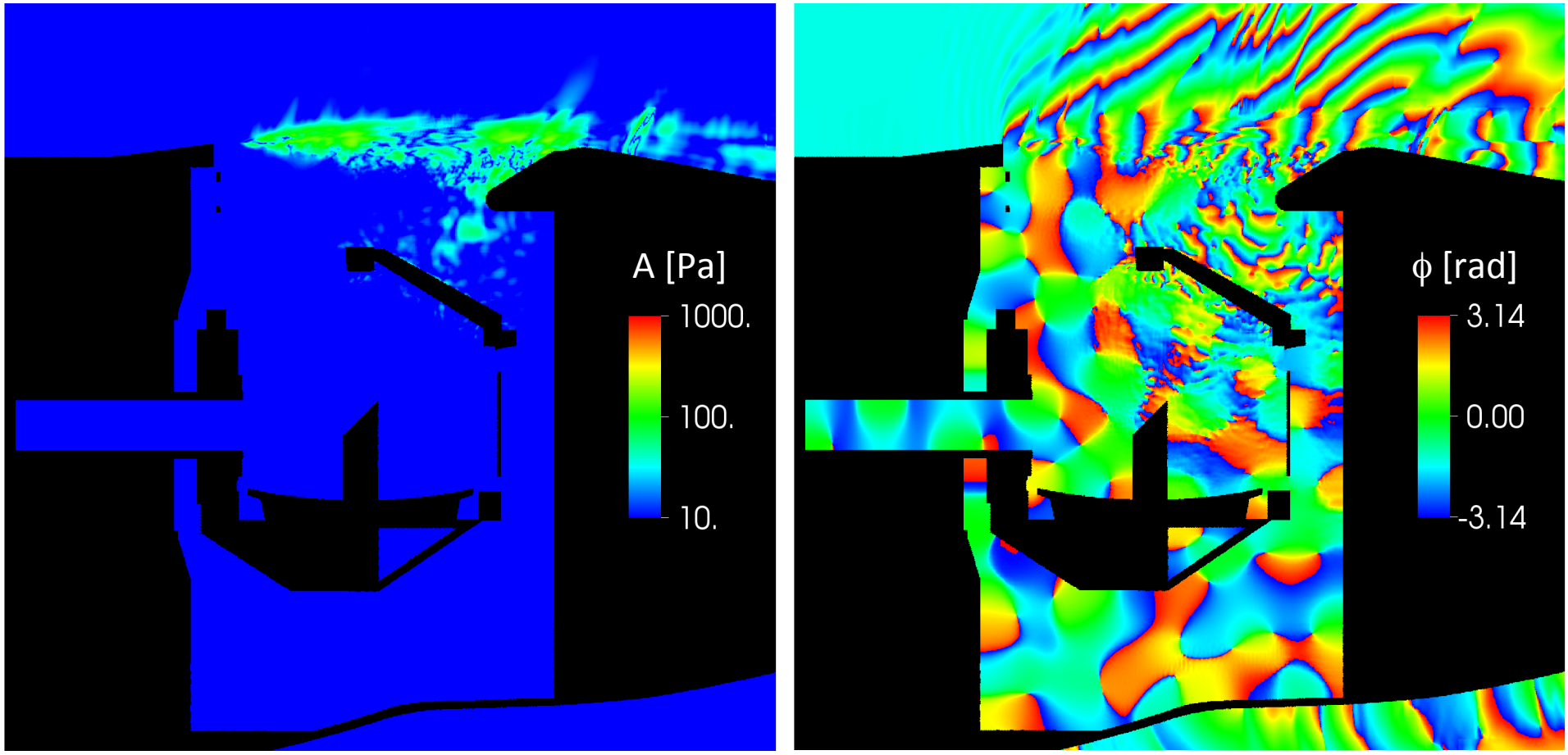

High amplitudes inside shear layer. Acoustic radiation away from shear layer. Complicated wave phase pattern inside cavity due to reflecting low amplitude acoustic waves.

Spectral Analysis at 1004 Hz

Amplitude [Pa]

Phase

A-B Plane

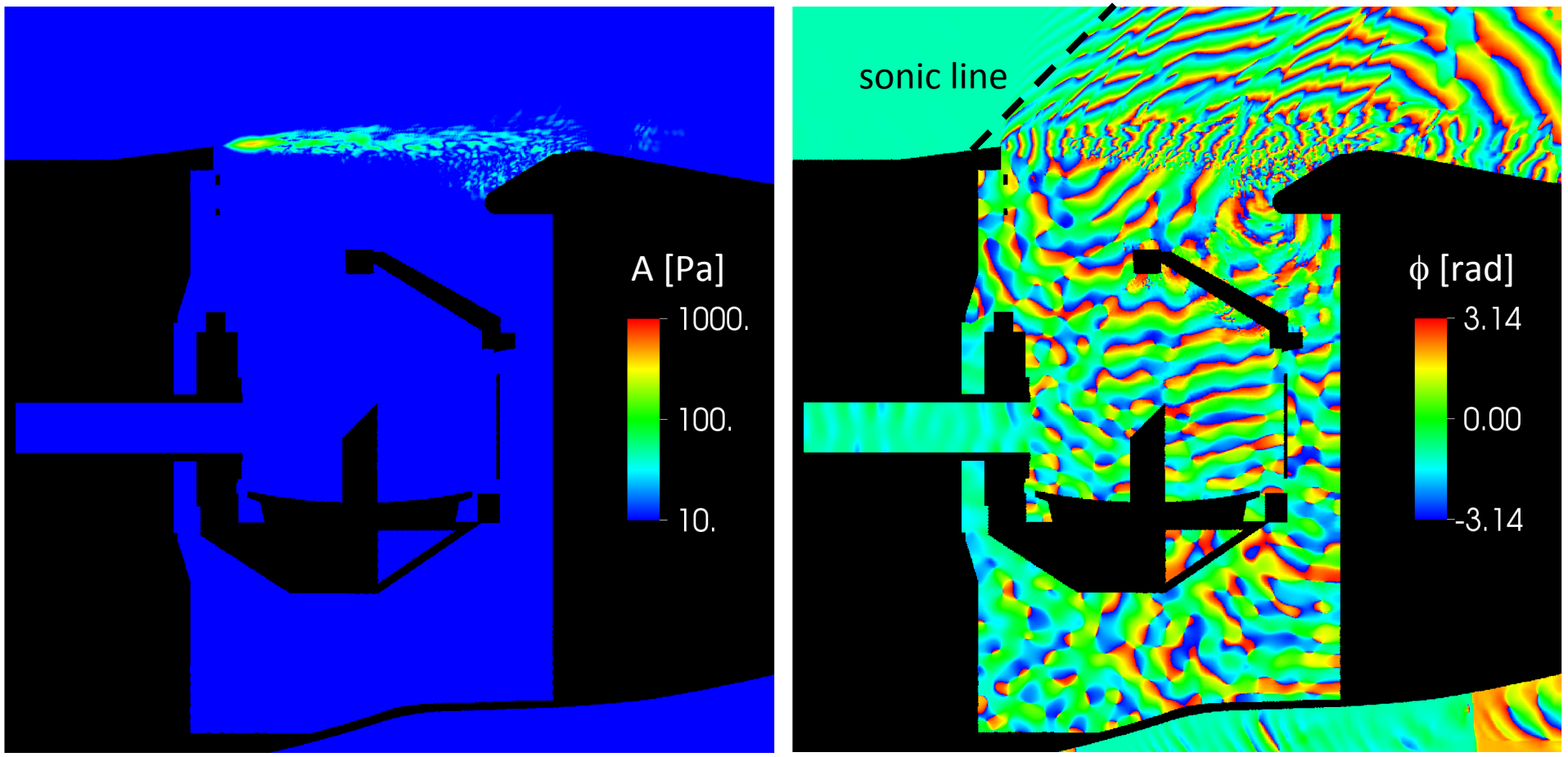

High amplitudes inside shear layer related to KH-instability (planar wave fronts in phase plot) with small wavelength. Downstream propagation outside of shear layer.

Outline

- Background/Motivation
- LAVA Solver
- SOFIA Simulation Setup
- General Flow Features
- Spectral Analysis
- Proper Orthogonal Decomposition Analysis
- Conclusions

Proper Orthogonal Decomposition

- **POD** results in a decomposition of the flow field into a set of basis functions that capture most of the flow energy as defined by a user-defined norm with the least number of modes*

$$\vec{q}(\vec{x},t) \approx \sum_{n=0}^{I} a^{(n)}(t)\vec{\chi}^{(n)}(\vec{x})$$

  - Used snapshot method** in temporal domain
  - Vector norm (energy) with

$$|\vec{q}|^2 = \int_V \left(\sum_{k=1}^{N_q} \omega_k \, q_k q_k \right) d\vec{x}$$

q_k=[p,u,v,w,$T^{0.5}$] and ω_k=[1,0,0,0,0]

*Rowley(2001), Freund and Colonius (2002)
**Lumley(1967), Sirovich (1987), Chatterje (2004)
***Nonomura et al (2011)

Proper Orthogonal Decomposition

Coarse Mesh

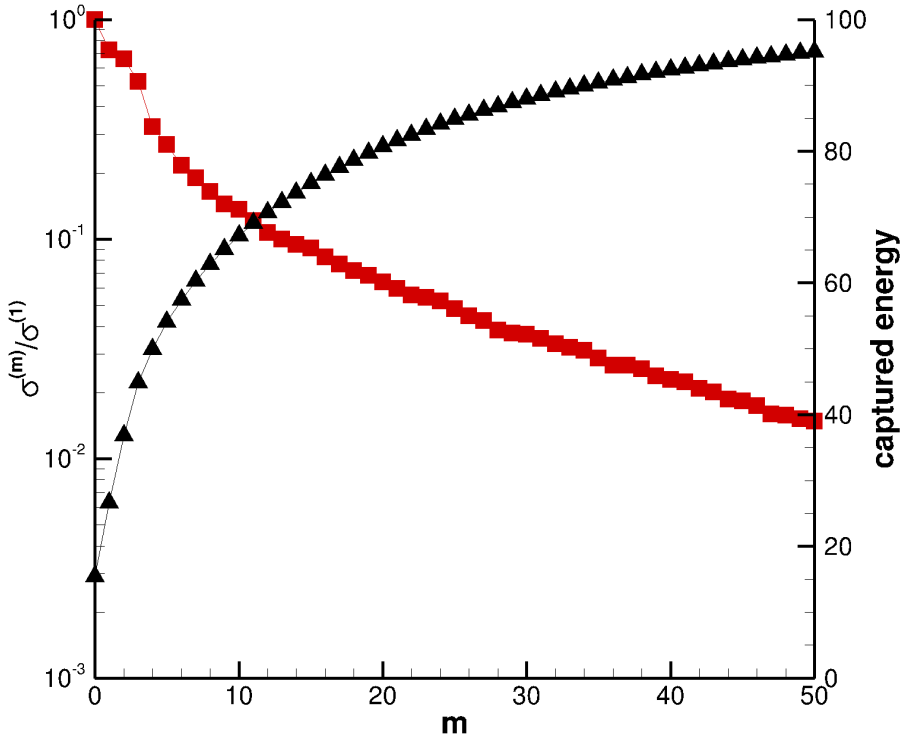

Fine Mesh

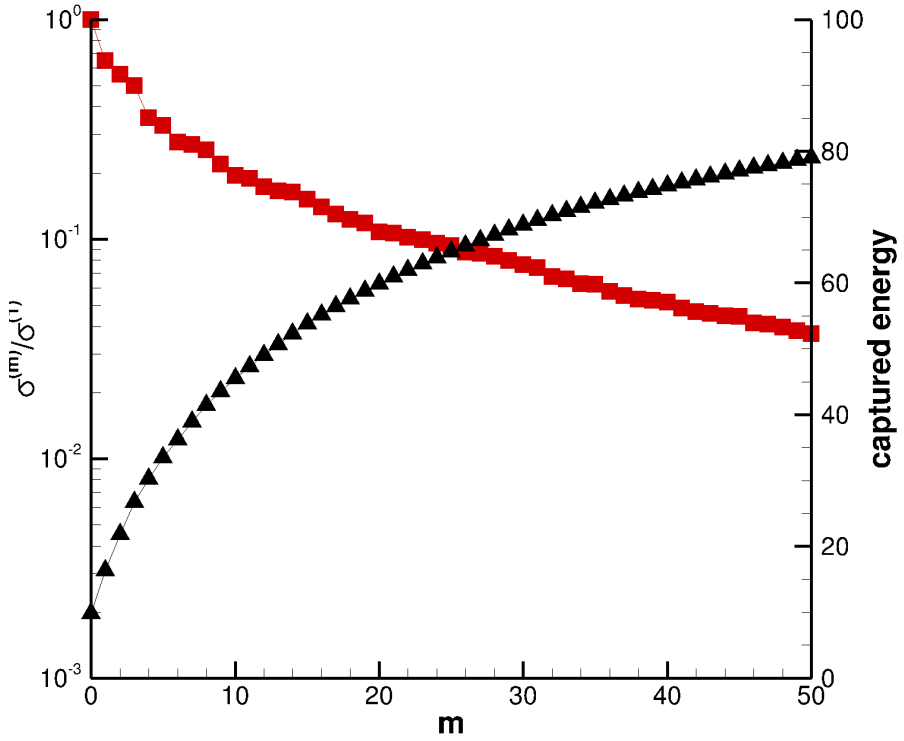

Singular value (red) relates to energy captured by mode (m).
Captured energy (black) = sum of mode energies (m).
Energy more evenly distributed for higher resolution simulation (50 modes capture only 80% of the total energy vs ~95% on coarse mesh) ➔ characteristic for highly turbulent flows

Proper Orthogonal Decomposition: Time Coefs

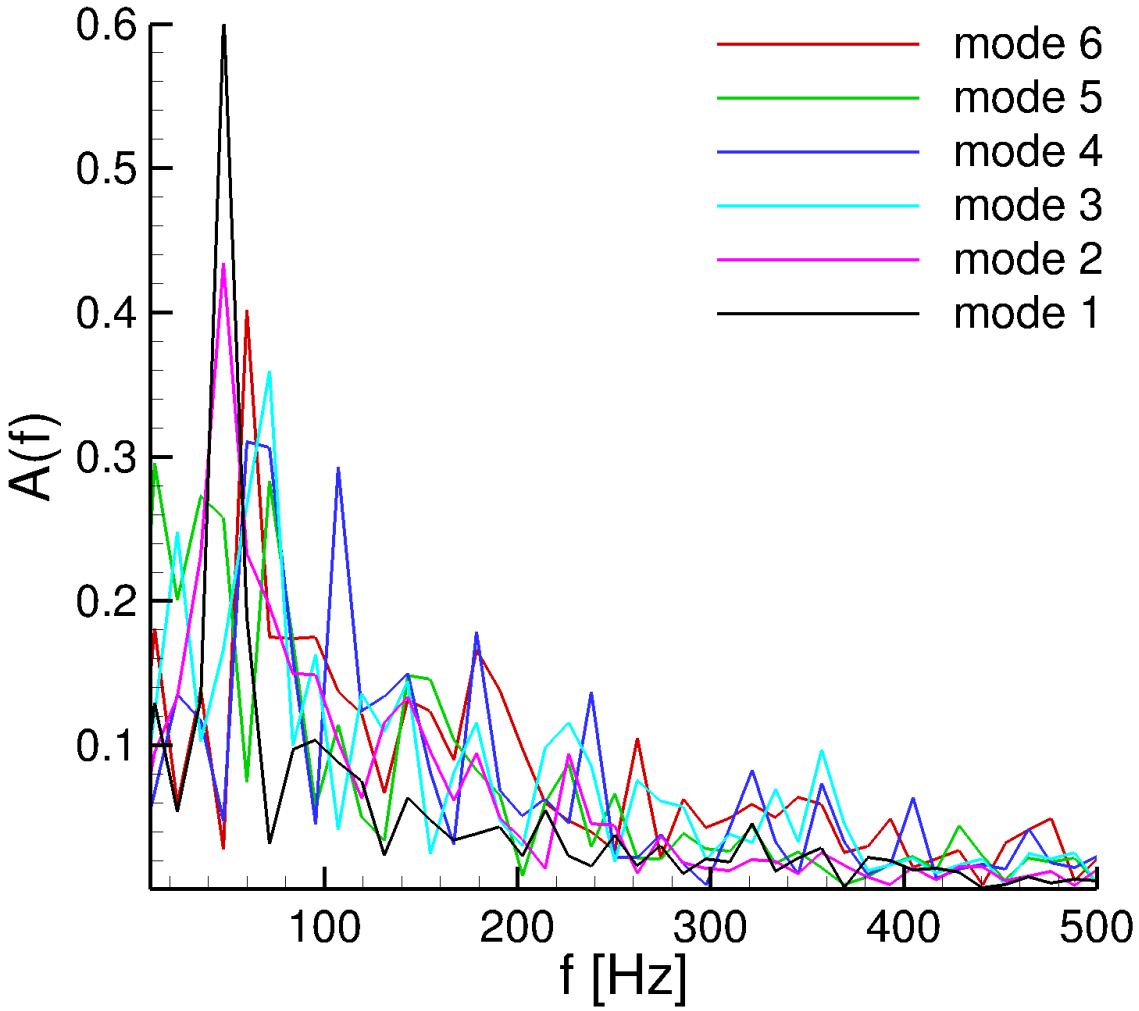

POD is able to capture cross frequency coupling (e.g. harmonics in mode 4)
Spectral characteristics of most energetic POD modes. Mode 1 shows isolated large amplitude for single low frequency. All other top six modes show high peak for low frequency < 100.

Proper Orthogonal Decomposition: Mode 1

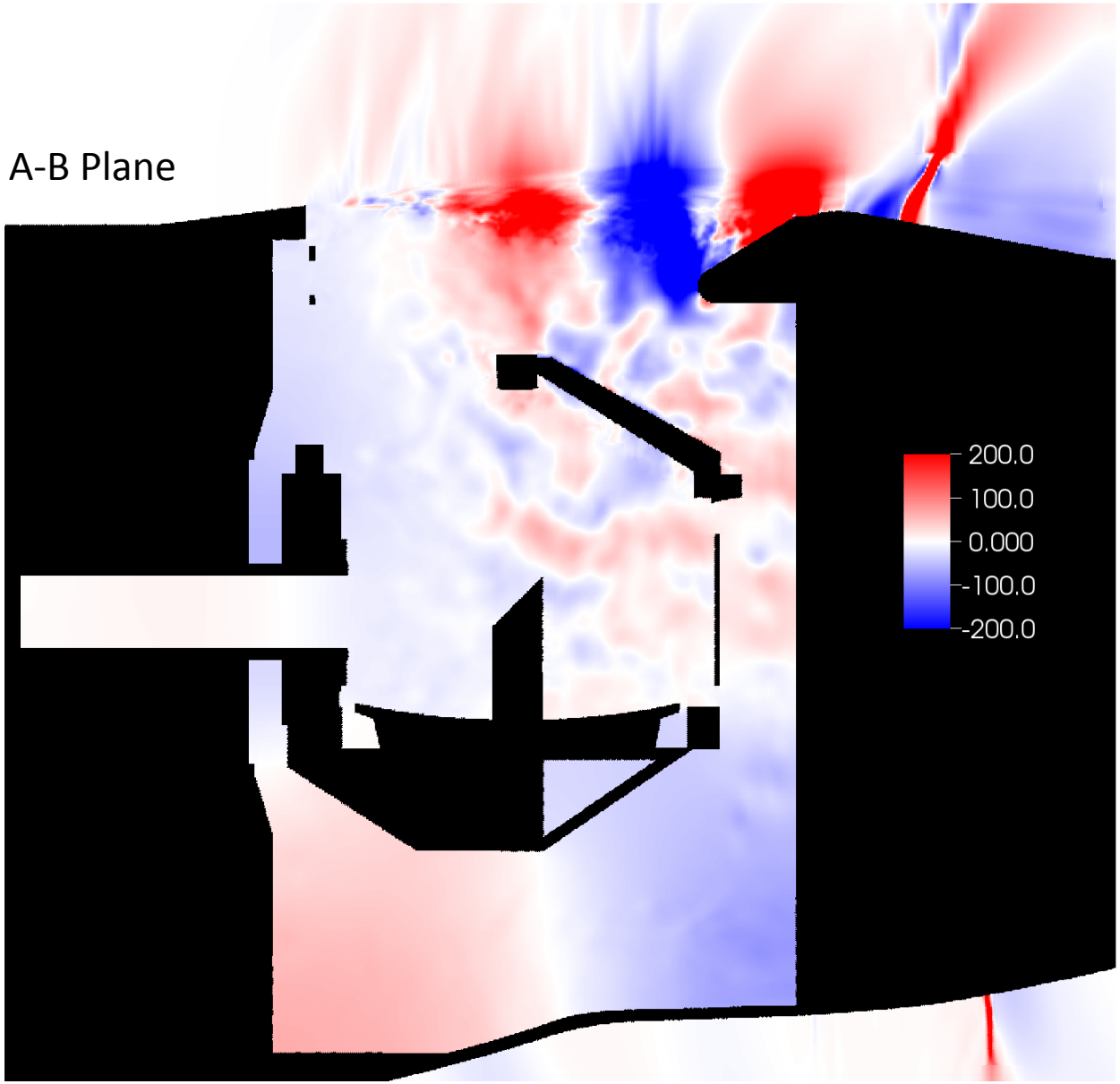

POD mode shape (red-white-blue color contours) only provides information about spatial distribution of unsteady pressure field. Singular value provides amplitude information (see two slides earlier). Unsteady pressure field can be reconstructed.

Mode 1 captures cavity mode which is coupled to unsteady pressure in shear layer. Coupling with shock.

Proper Orthogonal Decomposition: Mode 2

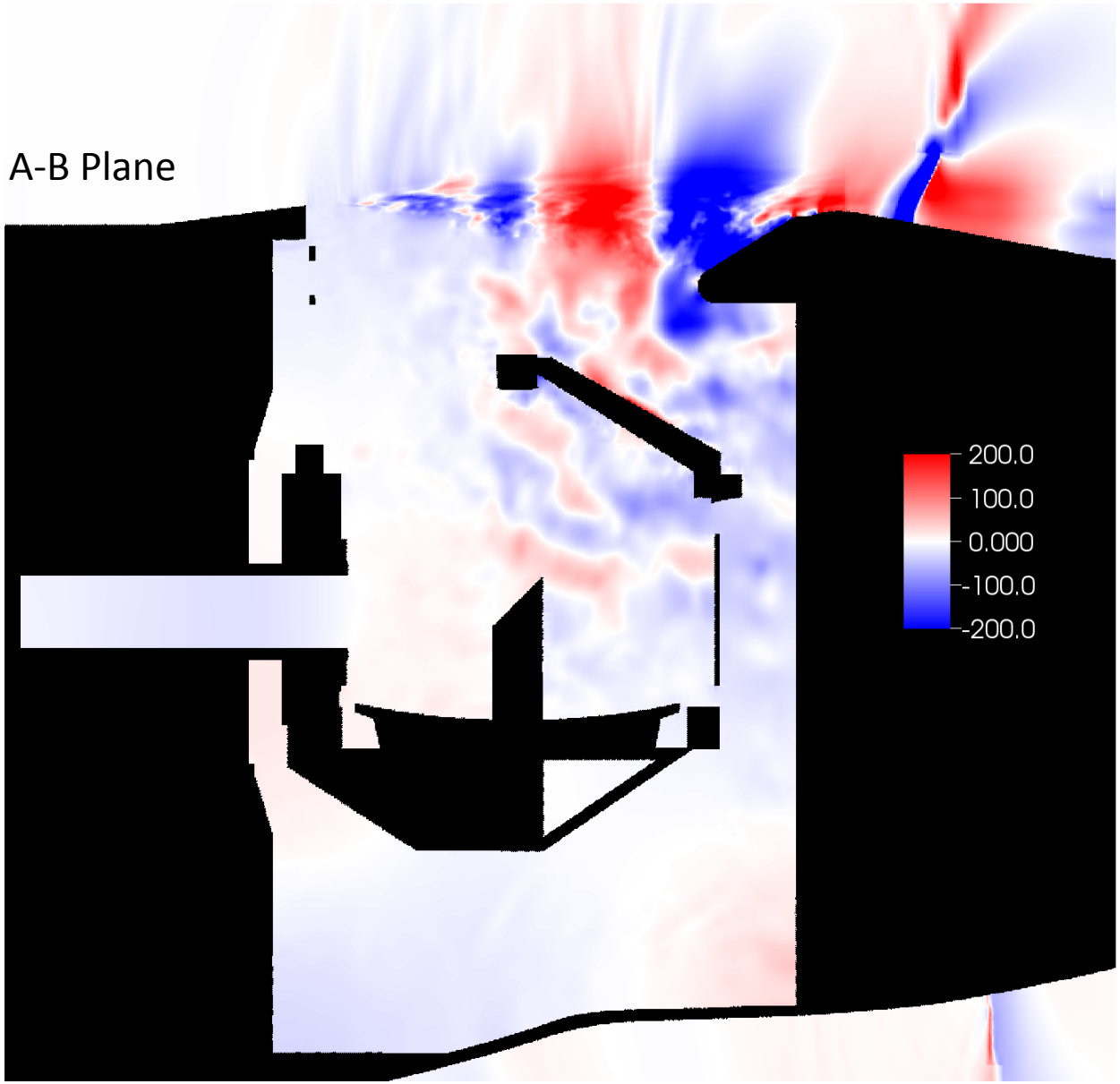

Mode 2 is dominant in shear layer and some presence in cavity can be observed. Coupling with shock.

Proper Orthogonal Decomposition: Mode 3

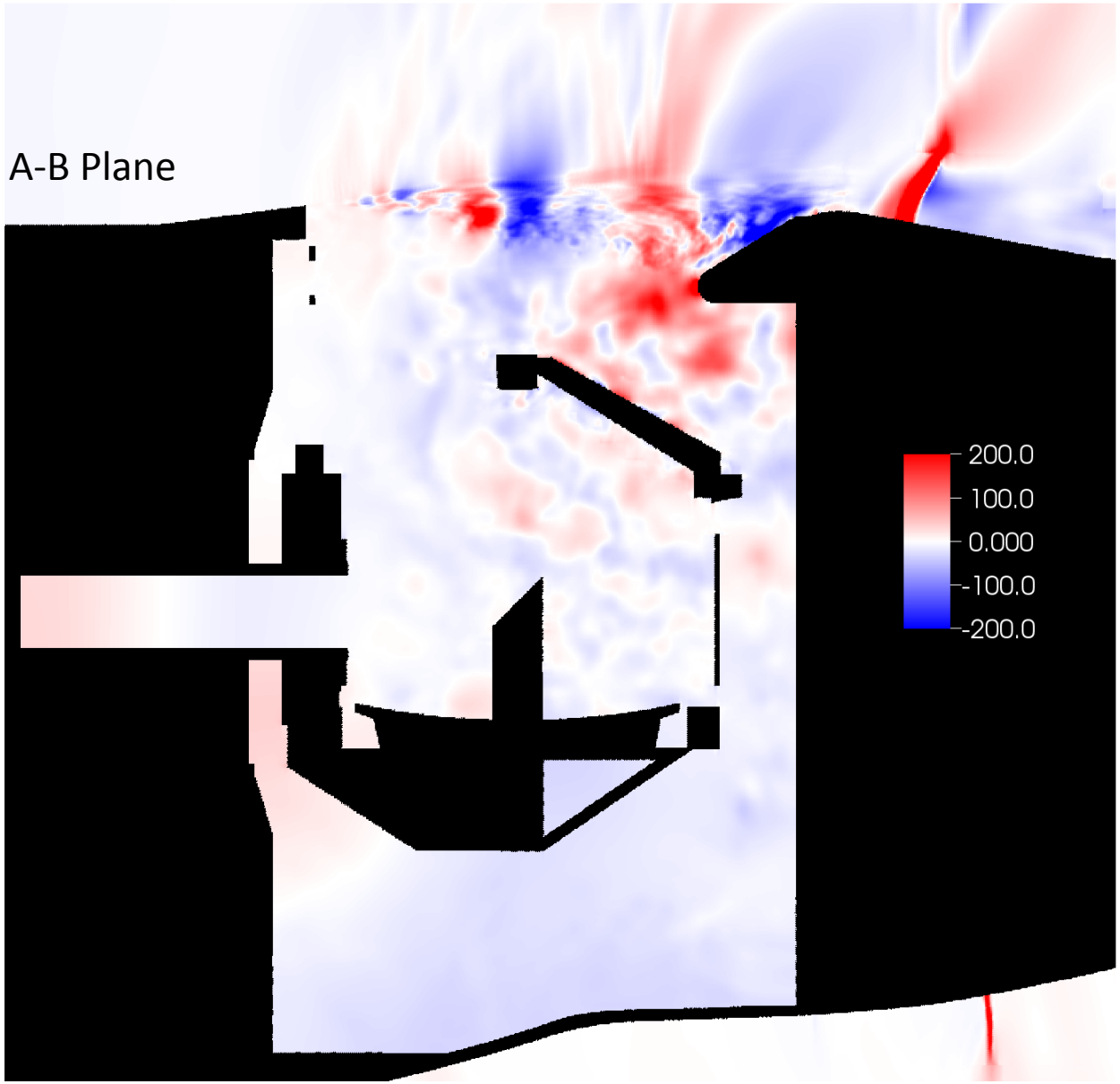

Modes 3-6 are similar to previous modes: most dominant in shear layer and some coupling to cavity mode. Coupling with shock.

Proper Orthogonal Decomposition: Mode 4

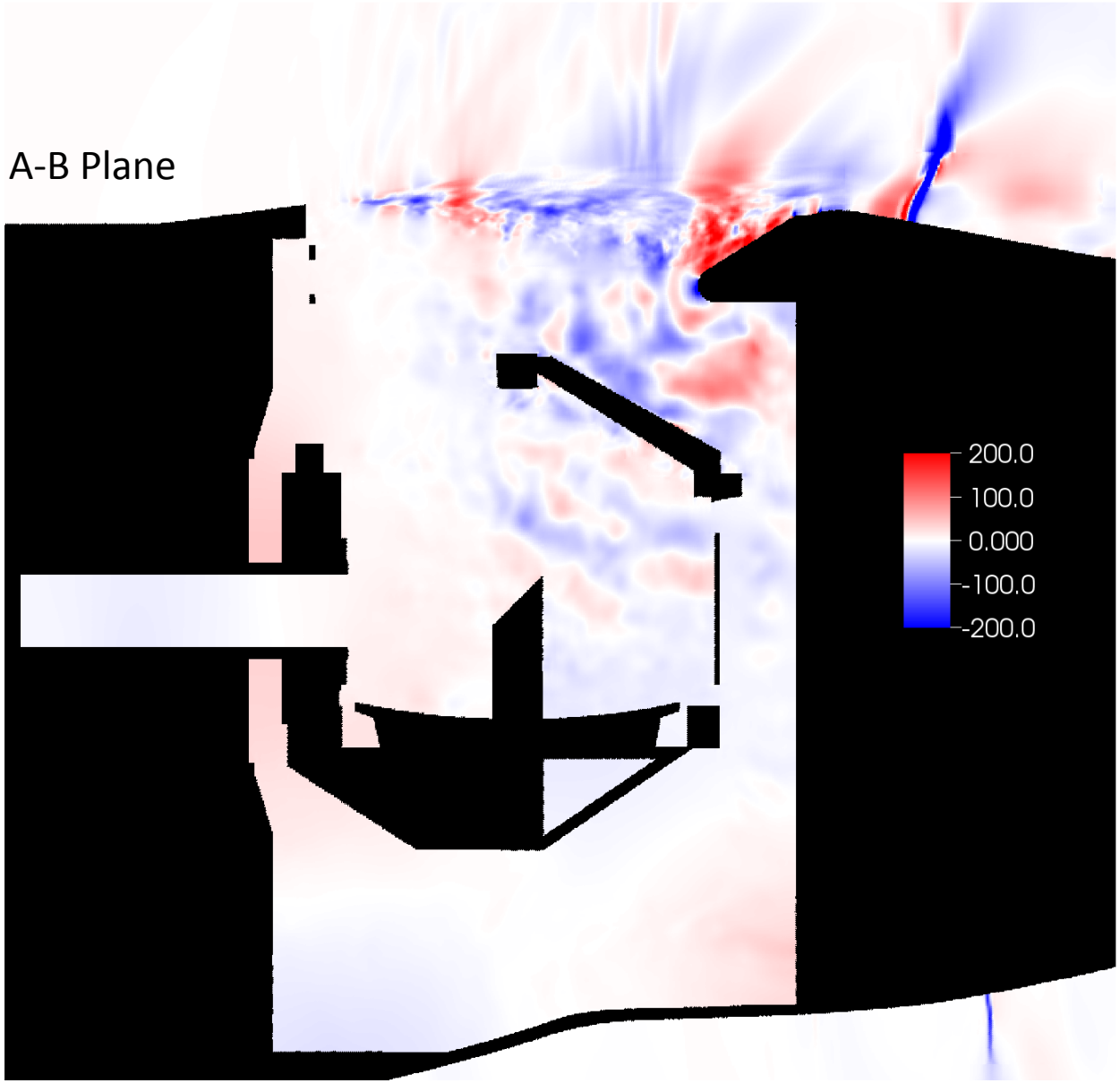

Modes 3-6 are similar to previous modes: most dominant in shear layer and some coupling to cavity mode. Coupling with shock.

Proper Orthogonal Decomposition: Mode 5

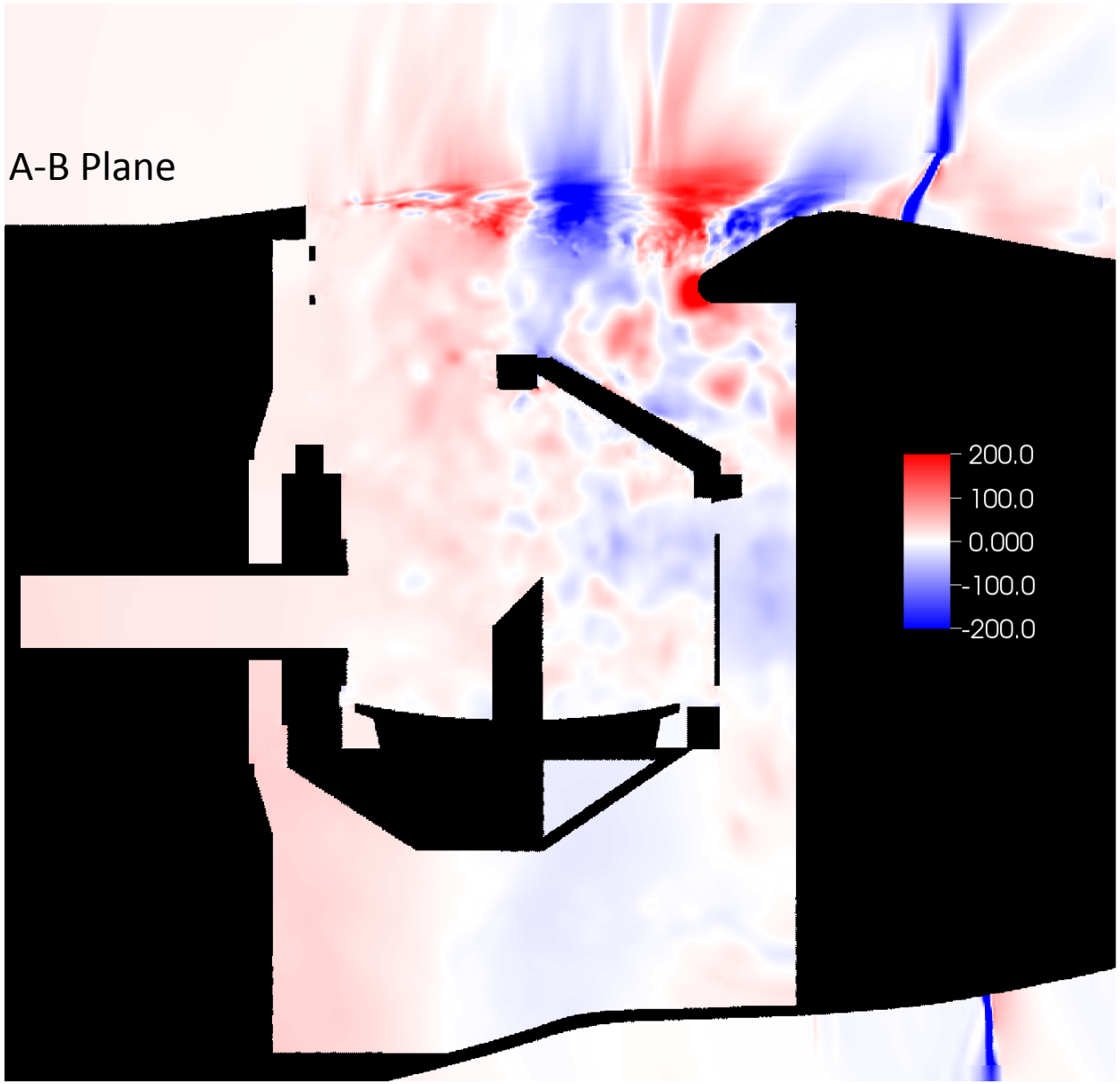

Modes 3-6 are similar to previous modes: most dominant in shear layer and some coupling to cavity mode. Coupling with shock.

Proper Orthogonal Decomposition: Mode 6

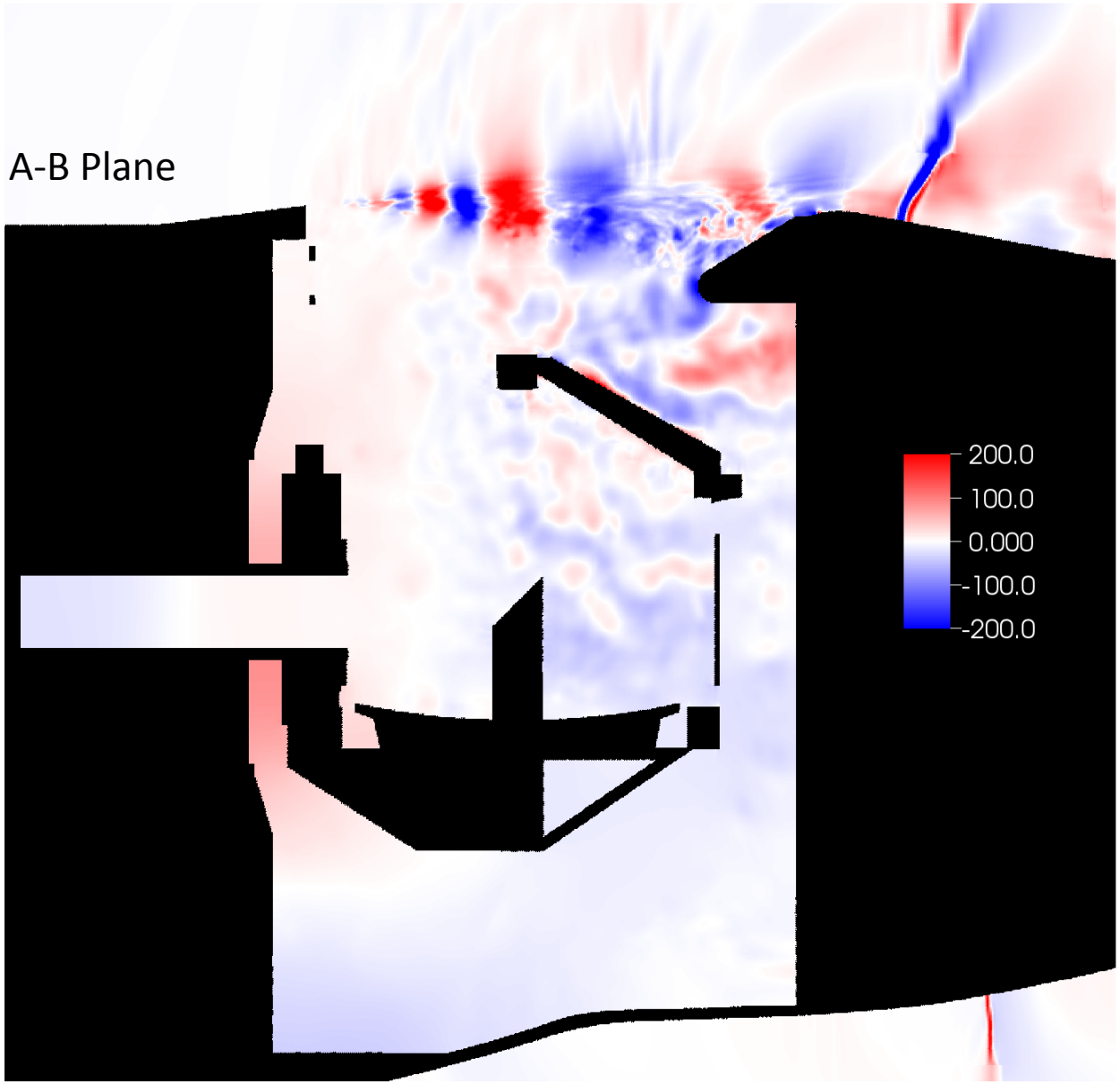

Modes 3-6 are similar to previous modes: most dominant in shear layer and some coupling to cavity mode. Coupling with shock.

Summary

- Summary
  - State-of-the-art simulation results demonstrate capabilities
    - Unsteady higher-order with shock capturing, grid flexibility, wall modeling, scalability, etc.
  - Post processed data provides insight into ongoing flow physics
    - Shear layer breakdown
    - Coupling between cavity mode and impinging shear layer
  - Spectral and POD analyses suggest that unsteady flow field is well captured
- Future
  - Fluid structure interaction
  - Detailed validation with flight/experimental data
  - Unsteady load integration on critical hardware
  - Shape optimization

Acknowledgments

- SOFIA Project for their support
- NASA Advanced Supercomputing (NAS) division
- LAVA Team (Emre Sozer, Shayan Moini-Yekta, Jeff Housman)
- Derrick Yabut (Summer Intern) & Henry Lee (STC Inc.)

Questions ?